Supporting information for

Exploring the Influence of Acceptor-Strength in Alkoxyphenanthrene-based A-π-D-π-A versus D-π-A Architectures for Resistive *WORM* Memory Devices

*Senthilkumar V Swetha,[a] Murali Ardra, [a] Predhanekar Mohamed Imran,[b] and Samuthira Nagarajan[a]**

[a]Organic Electronics Division, Department of Chemistry, Central University of Tamil Nadu, Thiruvarur-610 005, India, E-mail: snagarajan@cutn.ac.in

[b]Department of Chemistry, Islamiah College, Vaniyambadi, Chennai-635 752, India

Table of contents

1. General information

9,10-Phenanthroquinone, N-iodoscuccinimide, trifluromethane sulfonic acid, 1-bromohexane, sodium dithionite, 5-bromoisatin, o-phenylenediamine, 4-bromo-1,2-phenylenediamine, 2-methylbut-3-yn-2-ol, potassium carbonate, Bu_4NBr, KOH, $Pd(PPh_3)_2Cl_2$, and copper iodide were used as received from the commercial sources. ACS-grade solvents were used for spectroscopic analysis.

NMR spectra were acquired on a Bruker AVIII400 (400 MHz) spectrometer and were referenced to TMS, using $CDCl_3$/DMSO-d_6 as solvent. Chemical shifts (δ) are reported in parts per million (ppm), with signal splitting recorded as singlet (s), doublet (d), triplet (t), quartet (q), and multiplet and unresolved peaks (m). Coupling constants (*J*) are mentioned in Hz and are presented as observed. High-resolution mass spectra were obtained from Thermo Exactive Plus UHPLC-MS. Absorption and emission spectra were recorded using the JASCO UV-NIR spectrophotometer and Perkin-Elmer LS 55 spectrophotometer. Electrochemical studies were performed in a CHI electrochemical workstation (CHI 6035D). A conventional cell setup containing three electrodes was used with glassy carbon (working electrode), a standard calomel electrode (reference), and a platinum wire as the counter electrode in an anhydrous N,N-dimethylformamide solvent with tetrabutylammoniumhexafluorophosphate (Bu_4NPF_6) as a supporting electrolyte. The experiments were performed in an inert atmosphere with scan rates of 100 mV/s. Ferrocene/ferrocenium ion redox couple was used as the internal standard (4.8 eV below vacuum), and its redox potential is 0.44 V vs. SCE. The HOMO and LUMO energy levels were calculated from the onset of the oxidation/reduction potentials ($\varphi_{ox}/\varphi_{red}$) using the following equations: $E_{HOMO} = -e(\varphi_{ox} + 4.8)$ (eV); $E_{LUMO} = -e(\varphi_{red} + 4.86)$ (eV) where the unit of $\varphi_{ox}/\varphi_{red}$ is V vs. SCE. SEM measurements were performed with a VEGA 3 TESCAN microscope. Grazing incidence X-ray diffraction was performed in the reflection mode (CuKα radiation) by an XPERTPRO X-ray diffractometer. DFT studies were employed to analyze the geometry and energy levels of the molecules.

2. Synthetic route for the compounds 1-11

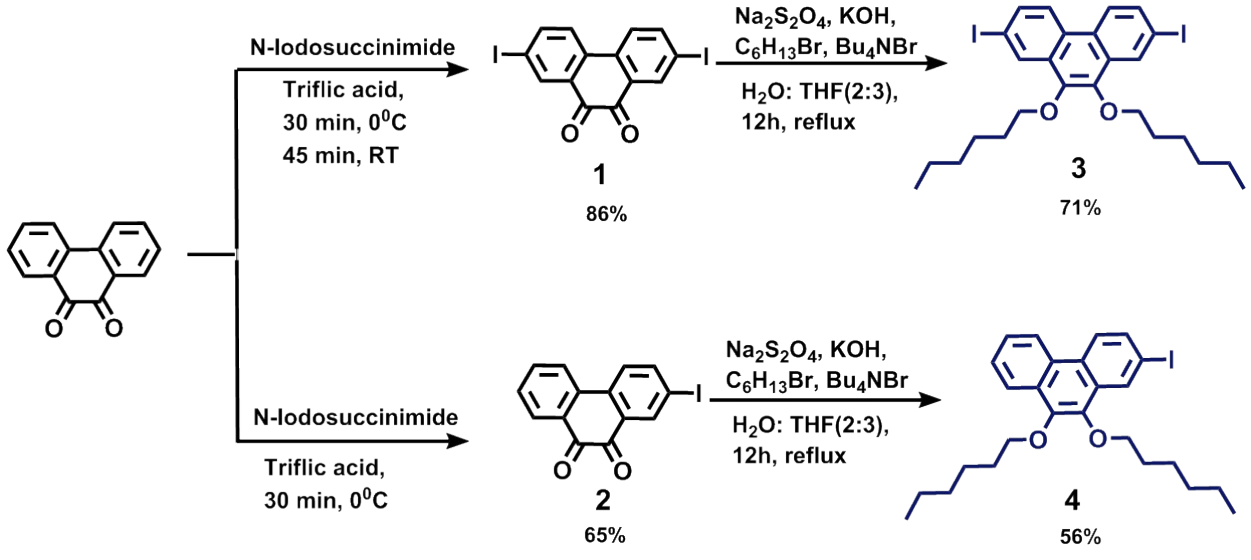

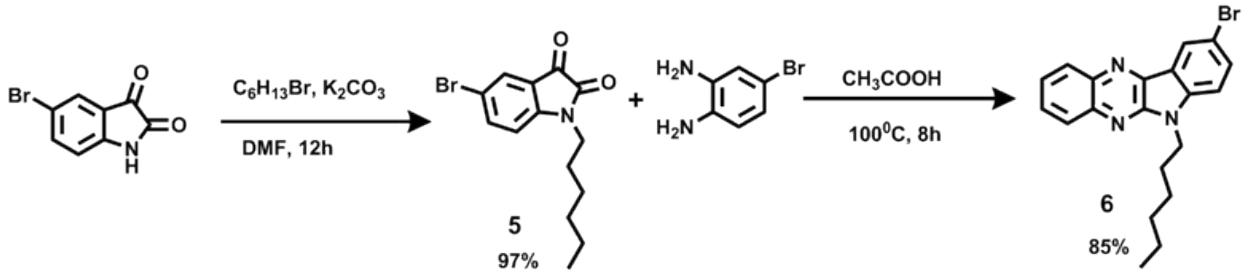

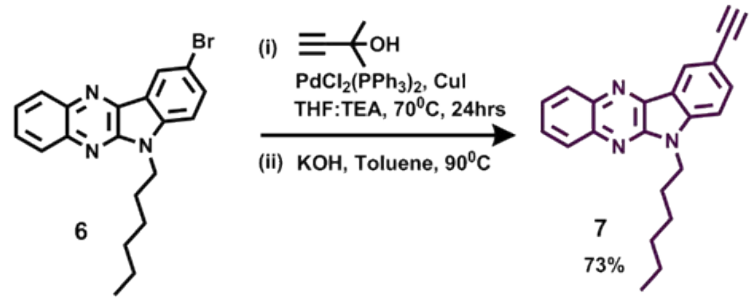

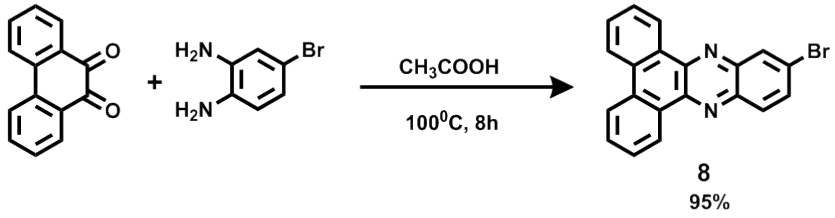

Scheme S1. Synthetic routes for compounds **1-9**

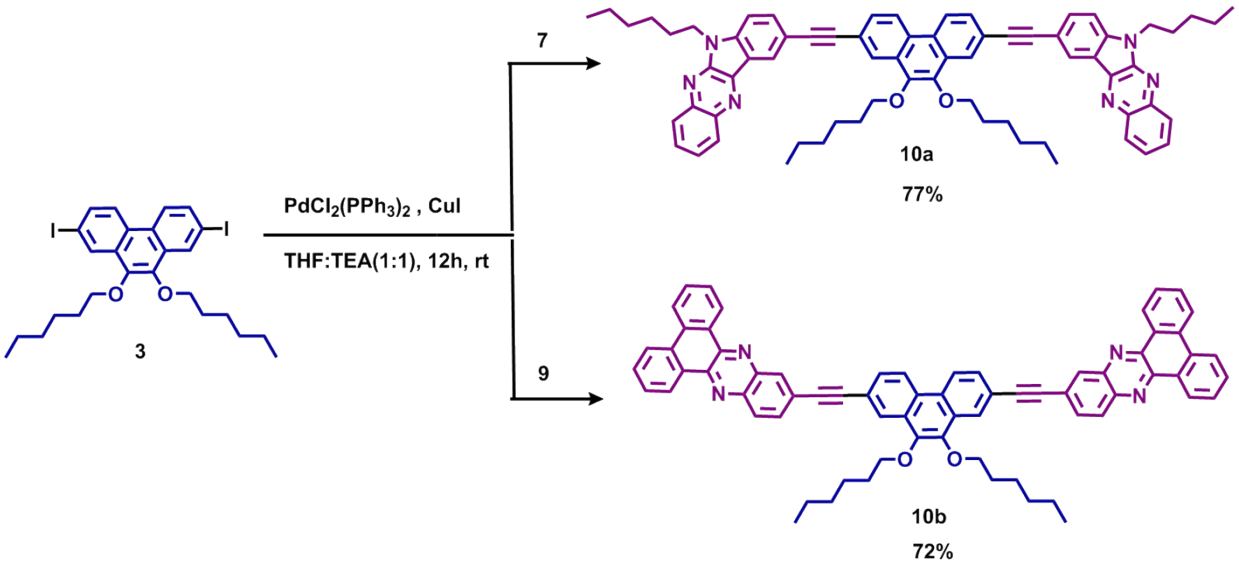

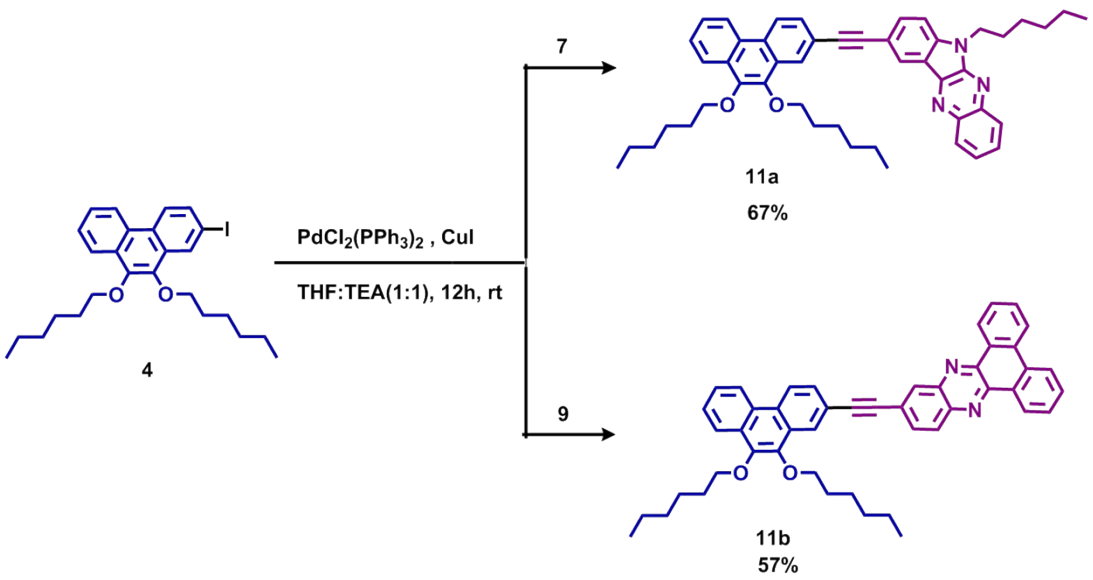

Scheme S2. Synthetic routes for compounds **10a-b** and **11a-b**

3. Synthetic and analytical data of compounds 1-11

Compound 1: Phenanthrene-9,10-dione (3.0 g, 14.4 mmol, 1.0 eq.) in trifluoromethane sulfonic acid (30 mL) was cooled to 0℃. N-Iodosuccinimide (9.75 g, 43.2 mmol, 3 eq) was added slowly to the reaction mixture for 30 minutes. Then, it was allowed to stir at room temperature for another 45 minutes, and the reaction mixture was added over H_2O to induce the precipitation. 2,7-Diiodophenanthrene-9,10-dione **1** was recrystallized from $CHCl_3$ and yielded 86 % as dark orange crystals.

Compound 2: Phenanthrene-9,10-dione (3.0 g, 14.4 mmol, 1.0 eq.) in trifluoromethane sulfonic acid (30 mL) was cooled to 0℃. N-iodosuccinimide (4.875 g, 21.6 mmol, 1.5 eq) was added slowly to the reaction mixture for 30 minutes. Then, it was allowed to settle to room temperature, and the reaction mixture was added to H_2O to induce the precipitation. 2-iodophenanthrene-9,10-dione **1** was recrystallized from $CHCl_3$ and yielded 65 % as orange crystals.

Compound 3: A mixture of compound **1** (5 g, 24.0 mmol), $Na_2S_2O_4$ (22.78 g, 144 mmol), and Bu_4NBr (4.64 g, 14.4 mmol) in 200 mL THF: H_2O (1:1, v/v) solvent was stirred for 15 minutes at room temperature. To this mixture, 1-bromohexane (8.98 g, 36 mmol), followed by aqueous KOH (20 g, 360 mmol, in 100 mL of H2O), was added slowly and stirred for another 48 hrs. The reaction mixture was diluted with 150 mL of water and then extracted with ethyl acetate (200 mL x 2). The combined organic layer was washed with water and brine, and then the solvent was removed under reduced pressure. The crude was recrystallized from methanol to yield compound **3** with a yield of 71%**.** ^{1}H NMR (400 MHz, $CDCl_3$) δ (ppm): 8.58 (d, J = 8 Hz, 2H), 8.27 (d, J = 8 Hz, 2H), 7.86-7.84 (m, 2H), 4.18 (t, 4H), 1.92-1.85 (m, 4H), 1.41-1.39 (m, 12H), 0.96-0.92 (m, 6H). ^{13}C NMR (100 MHz, $CDCl_3$) δ (ppm): 142.58, 134.54, 131.44, 127.08, 124.07, 93.28, 73.72, 31.67, 30.33, 29.72, 25.89, 22.72, 14.10.

Compound 4: A mixture of compound **2** (5 g, 24.0 mmol), $Na_2S_2O_4$ (22.78 g, 144 mmol), and Bu_4NBr (4.64 g, 14.4 mmol) in 200 mL THF: H_2O (1:1, v/v) solvent was stirred for 15 minutes at room temperature. To this mixture, 1-bromohexane (8.98 g, 36 mmol), followed by aqueous KOH (20 g, 360 mmol, in 100 mL of H2O), was added slowly and stirred for another 48 hrs. The reaction mixture was diluted with 150 mL of water and then extracted with ethyl acetate (200 mL x 2). The

combined organic layer was washed with water and brine, and then the solvent was removed under reduced pressure. The crude was recrystallized from methanol to yield compound **4,** yielding 56 % as an off-white solid**.** ^{1}H NMR (400 MHz, $CDCl_3$) δ 8.51-8.45 (m, 2H), 8.15-8.13 (m, 2H), 7.62-7.73 (m, 2H), 7.56-7.49 (m, 1H), 4.12-4.06 (m, 4H), 1.83-1.79 (m, 4H), 1.51-1.46 (m, 4H), 1.33-1.28 (m, 8H), 0.86-0.82 (m, 6H). ^{13}C NMR (100 MHz, $CDCl_3$) δ 143.95, 142.69, 141.92, 134.54, 134.17, 131.38, 129.70, 128.72, 127.81, 127.26, 125.99, 124.67, 123.96, 122.28, 93.56, 92.77, 73.86, 31.74, 30.11, 29.96, 25.91, 22.68, 14.13.

Compound 5: 5-Bromoisatin (4.42 mmol, 1.0 g) was dissolved in DMF at 0°C, and after 5 minutes of stirring, potassium carbonate (8.84 mmol, 1.22 g) was added. The mixture was stirred for 1 hr at 0°C. The reaction mixture colour transformed to wine red. 1-Bromohexane (4.42 mmol, 0.73 g) was added to the reaction mixture and stirred at room temperature for 12 hours. The resultant mixture was poured over ice water and extracted with dichloromethane. The combined organic phase was dried over anhydrous Na_2SO_4, and the solvent was removed under reduced pressure. The crude was purified by column chromatography on silica gel (EtOAc: hexane) to afford compound **5** with a yield of 97 % as red crystals. ^{1}H NMR (400 MHz, $CDCl_3$) δ (ppm): 7.73-7.67 (m, 2H), 6.81 (d, J = 7.9 Hz, 1H), 3.74-3.68 (m, 2H), 1.71-1.64 (m, 2H), 1.38-1.30 (m, 6H), 0.889 (t, J = 7.0 Hz, 3H). ^{13}C NMR (100 MHz, $CDCl_3$) δ (ppm): 182.52, 157.41, 149.77, 140.51, 128.26, 118.79, 116.43, 111.85, 40.43, 31.35, 27.13, 26.53, 22.50, 13.99.

Compound 6: Compound **5** (3.23 mmol, 1.0 g) and o-phenylenediamine (0.35 g, 1 eq) were dissolved in acetic acid and refluxed for 8 hours. The resultant mixture was poured over ice water and extracted with dichloromethane. The combined organic phase was dried over Na_2SO_4, and the solvent was removed under reduced pressure. The crude was purified by column chromatography on silica gel (EtOAc/hexane) to afford compound **6** as a yellow solid with a yield of 95 %. ^{1}H NMR (400 MHz, $CDCl_3$) δ (ppm): 8.60 (s, 1H), 8.28 (d, J = 8 Hz, 1H), 8.13 (d, J = 8 Hz, 1H), 7.77 (t, J = 8 Hz, 2H), 7.69 (t, J = 8 Hz, 1H), 7.35 (d, J = 8 Hz, 1H). ^{13}C NMR (100 MHz, $CDCl_3$) δ (ppm): 145.50, 142.91, 140.87, 139.37, 133.36, 129.44, 129.15, 127.89, 126.33, 125.41, 121.07, 113.52, 110.98, 41.58, 31.46, 28.41, 26.70, 22.55, 14.03.

Compound 8: A mixture of phenanthrene-9,10-dione (1g, 4.80 mmol) and 4- bromobenzene-1,2-diamine (0.98 g, 5.28 mmol) in acetic acid (20 mL) was refluxed for 8 hours. After completion,

the reaction mixture was cooled to room temperature and poured into ethanol, followed by filtration of the crude product. The solid was washed with ethanol several times. The crude product was purified by column chromatography on silica gel using a hexane: ethyl acetate system and dried under reduced pressure to give **8** as a yellow solid in 84 % yield. ^{1}H NMR (400 MHz, $CDCl_3$) δ (ppm): 9.36 (d, *J* = 8 Hz, 2H), 8.57 (d, *J* = 8 Hz, 2H), 8.52 (s, 1H), 8.19 (d, *J* = 8.8 Hz, 1H), 7.92 (d, *J = 9.0 Hz*, 1H), 7.86 – 7.71 (m, 4H); ^{13}C NMR (100 MHz, $CDCl_3$) δ (ppm): 142.99, 142.65, 142.53, 140.79, 133.30, 132.26, 132.11, 131.56, 130.71, 130.69, 130.59, 130.00, 129.93, 128.06, 126.40, 126.35, 126.28, 123.79, 122.98, 122.96.

General synthesis procedure for Sonagashira cross-coupling reaction

In a two-necked round bottom flask, aryl halide in dry THF (10 mL) and Et_3N (20 mL), followed by $PdCl_2(PPh_3)_2$ (0.05 mol% %), CuI (0.05 mol%), was taken under nitrogen. Corresponding acetylene was introduced after 10 minutes. The progress of the reaction was monitored by thin-layer chromatography. After the completion of the reaction, the organic phase was separated using dichloromethane, and the solvent was removed under reduced pressure. The crude was purified by column chromatography using silica gel 100-200 mesh and ethyl acetate/hexane as stationary and mobile phases, respectively.

Compound 7: A mixture of **6** (1 g, 2.62 mmol) in 1:2 dry THF: Et_3N, $PdCl_2(PPh_3)_2$ (0.09 g, 0.05 mol %) and CuI (0.25 g, 0.05 mol %) was allowed to react with 2-methylbut-3-yn-2-ol (0.35 g, 4.11 mmol) at 70℃ for 24 hours as per the general procedure for Sonagashira coupling reaction to afford 4-(6-hexyl-6H-indolo[2,3-b]quinoxalin-9-yl)-2-methylbut-3-yn-2-ol as a yellow solid. The resultant intermediate (0.72 g, 1.86 mmol) and KOH (2 equivalents) were dissolved in toluene and refluxed for 5 hours. The reaction mixture was poured over water and extracted with dichloromethane. The crude product was purified by column chromatography on silica gel (EtOAc: Hexane) to afford **7.** ^{1}H NMR (400 MHz, $CDCl_3$) δ (ppm): 8.53 (d, 1H), 8.24 (dd,1H), 8.10 (dd, 1H), 7.74-7.65 (m, 3H), 7.28 (d, *J* = 8 Hz*,* 1H), 4.39 (t, 2H), 3.12 (s, 1H), 1.92-1.85 (m, 2H), 1.36-1.34 (m, 6H), 0.86-0.83 (m, 3H). ^{13}C NMR (100 MHz, $CDCl_3$) δ (ppm): 171.18, 162.66, 141.52, 137.66, 132.40, 131.91, 130.31, 129.90, 129.22, 127.78, 126.16, 124.16, 122.12, 114.69, 111.92, 99.25, 97.04, 81.64, 65.56, 60.57, 36.31, 34.57, 31.43, 26.64, 22.54, 14.14.

Compound 9: A mixture of **8** (1 g, 2.62 mmol) in 1:2 dry THF: Et_3N, $PdCl_2(PPh_3)_2$ (0.09 g, 0.05 mol%) and CuI (0.25 g, 0.05 mol %) was allowed to react with 2-methylbut-3-yn-2-ol (0.35 g,

4.11 mmol) at 70°C for 24 hours as per the general procedure for Sonagashira coupling reaction to afford 4-(dibenzo[a,c]phenazin-11-yl)-2-methylbut-3-yn-2-ol as off-white solid. The resultant intermediate (0.72 g, 1.86 mmol) and KOH (2 equivalents) were dissolved in toluene and refluxed for 5 hours. The reaction mixture was poured over water and extracted with dichloromethane. The crude product was purified by column chromatography on silica gel (EtOAc: hexane) to afford **7.** ^{1}H NMR (400 MHz, $CDCl_3$) δ (ppm): 8.57 (s, 1H), 8.26 (d, *J* = 8 Hz, 1H), 8.12 (d, *J* = 8 Hz, 1H), 7.77-7.66 (m, 4H), 7.33-7.29 (m, 1H), 4.43 (s, 1H); ^{13}C NMR (100 MHz, $CDCl_3$) δ (ppm): 142.97, 142.86, 142.53, 141.42, 133.10, 132.84, 132.12, 131.57, 130.10, 129.53, 128.76, 127.51, 126.22, 123.48, 122.23, 84.65, 83.33, 79.41, 73.53, 22.54, 14.33.

Compound 10a: A mixture of **3** (0.63 g, 1 mmol), $PdCl_2(PPh_3)_2$ (0.05 mol%), and CuI (0.05 mol%) in a 1:1 mixture of dry THF: Et_3N was allowed to react with **7** as per the Sonogashira coupling reaction. The reaction mixture was stirred at room temperature for 24 hrs to afford **10a.** ^{1}H NMR (400 MHz, $CDCl_3$) δ (ppm): 8.75 (s, 2H), 8.58 (d, *J* = 8 Hz, 2H), 8.44 (d, *J* = 4 Hz, 2H), 8.33 (d, *J* = 8 Hz, 2H), 8.16 (d, *J* = 8 Hz, 2H), 7.92 (d, *J* = 8 Hz, 2H), 7.79-7.77 (m, 4H), 7.75-7.71 (m, 2H), 7.49 (d, *J* = 8 Hz, 2H), 4.49 (t, 4H), 4.27 (t, 4H), 1.98-1.63 (m, 8H), 1.48-1.33 (m, 12H), 1.33-1.25 (m, 12H), 0.99-0.96 (m, 6H), 0.88-0.85 (m, 6H). ^{13}C NMR (100 MHz, $CDCl_3$) δ (ppm): 146.09, 143.18, 141.53, 140.22, 137.17, 134.64, 133.77, 130.25, 127.57, 127.32, 125.68, 124.62, 123.43, 122.95, 117.94, 92.32, 89.21, 72.32, 35.56, 33.36, 30.63, 29.28, 28.34, 25.06, 21.68, 20.06, 12.76. HRMS (ESI) m/z: 1028.9371 $[M]^+$, calcd for $C_{70}H_{72}N_6O_2$; Found 1028.9578.

Compound 10b: A mixture of **3** (0.63 g, 1 mmol), $PdCl_2(PPh_3)_2$ (0.05 mol%), and CuI (0.05 mol%) in a 1:1 mixture of dry THF: Et_3N was allowed to react with **9** as per the Sonogashira coupling reaction. The reaction mixture was stirred at room temperature for 24 hrs to afford **10b.** ^{1}H NMR (400 MHz, $CDCl_3$) δ (ppm): 9.20 (d, *J* = 8 Hz, 4H), 8.75 (d, *J* = 8 Hz, 6H), 8.38-8.36 (m, 2H), 8.29-8.26 (m, 2H), 7.95-7.93 (m, 2H), 7.90-7.80 (m, 10H), 7.78-7.66 (m, 2H), 4.56 (t, 2H), 4.12 (t, 2H), 1.99-1.97 (m, 3H), 1.57-1.54 (m, 4H), 1.33-1.25 (m, 6H), 0.88-0.85 (m, 5H). ^{13}C NMR (100 MHz, $CDCl_3$) δ (ppm): 145.43, 142.84, 140.82, 139.32, 138.56, 134.51, 133.32, 129.41, 129.12, 127.87, 126.62, 125.94, 125.28, 122.71, 120.91, 113.39, 110.67, 83.68, 82.83, 41.55, 31.45, 29.72, 29.47, 28.43, 26.69, 22.55, 14.04**.** HRMS (ESI) m/z: 983.9741 $[M]^+$, calcd for $C_{70}H_{54}N_4O_2$; Found 983.9766.

Compound 11a: A mixture of **4** (0.32 g, 1 mmol), $PdCl_2(PPh_3)_2$ (0.05 mol%), and CuI (0.05 mol%) in a 1:1 mixture of dry THF: Et_3N was allowed to react with **7** as per the Sonogashira coupling reaction. The reaction mixture was stirred at room temperature for 24 hrs to afford **11a.** ^{1}H NMR (400 MHz, $CDCl_3$) δ (ppm): 8.62 (dd, 1H), 8.52-8.43 (m, 1H), 8.31-8.27 (m, 2H), 8.15-8.11 (m, 2H), 7.82 (dd, 1H), 7.76-7.74 (m, 5H), 7.72-7.67 (m, 2H), 4.47-4.26 (m, 6H), 1.98-1.89 (m, 6H), 1.46-1.22 (m, 18H), 0.99-0.95 (m, 3H), 0.88-0.83 (m, 6H); ^{13}C NMR (100 MHz, $CDCl_3$) δ (ppm): 171.18, 162.66, 141.52, 137.66, 132.40, 131.91, 130.31, 129.90, 129.22, 127.78, 126.16, 124.16, 122.12, 114.69, 111.92, 99.25, 97.04, 81.64, 77.39, 77.07, 76.76, 65.56, 60.57, 36.31, 34.57, 31.43, 29.15, 26.64, 22.54, 21.00, 20.97, 14.14. HRMS (ESI) m/z: 703.4221 $[M]^+$, calcd for $C_{48}H_{53}N_3O_2$; Found 703.4130.

Compound 11b: A mixture of **4** (0.32 g, 1 mmol), $PdCl_2(PPh_3)_2$ (0.05 mol%), and CuI (0.05 mol%) in a 1:1 mixture of dry THF: Et_3N was allowed to react with **9** as per the Sonogashira coupling reaction. The reaction mixture was stirred at room temperature for 24 hrs to afford **11b.** ^{1}H NMR (400 MHz, $CDCl_3$) δ (ppm): 9.38 (t, 2H), 8.59-8.52 (m, 5H), 8.52-8.47 (s, 1H), 8.47-8.26 (m, 2H), 7.86 (d, J = 8 Hz, 1H), 7.78-7.76 (m, 7H), 4.14 (m, 4H), 2.11-1.97 (m, 4H), 1.45-1.40 (m, 6H), 1.33-1.25 (m, 6H), 0.99-0.94 (m, 6H); ^{13}C NMR (100 MHz, $CDCl_3$) δ (ppm):143.34, 143.11, 142.90, 141.89, 134.47, 132.49, 132.16, 131.54, 131.38, 130.55, 128.72, 128.04, 127.19, 126.44, 126.21, 124.36, 123.04, 122.72, 93.58, 92.83, 90.13, 82.10, 80.69, 73.73, 31.85, 30.66, 25.95, 22.93, 20.12, 14.24. HRMS (ESI) m/z: 680.3101 $[M]^+$, calcd for $C_{48}H_{44}N_2O_2$; Found 680.3019.

4. ^{1}H and ^{13}C NMR spectra of the synthesized compounds

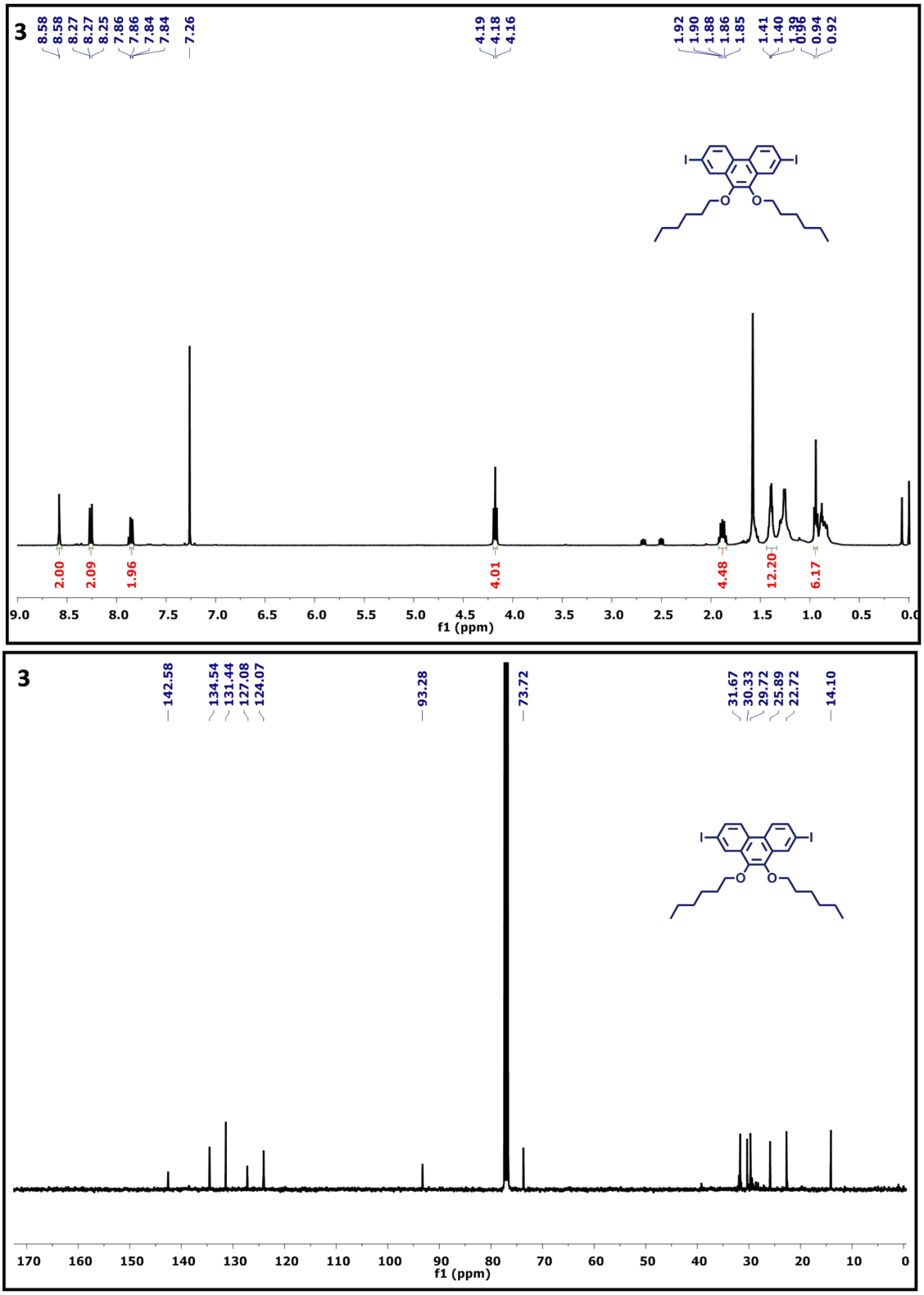

Figure S1: ^{1}H and ^{13}C NMR spectra of compound **3**

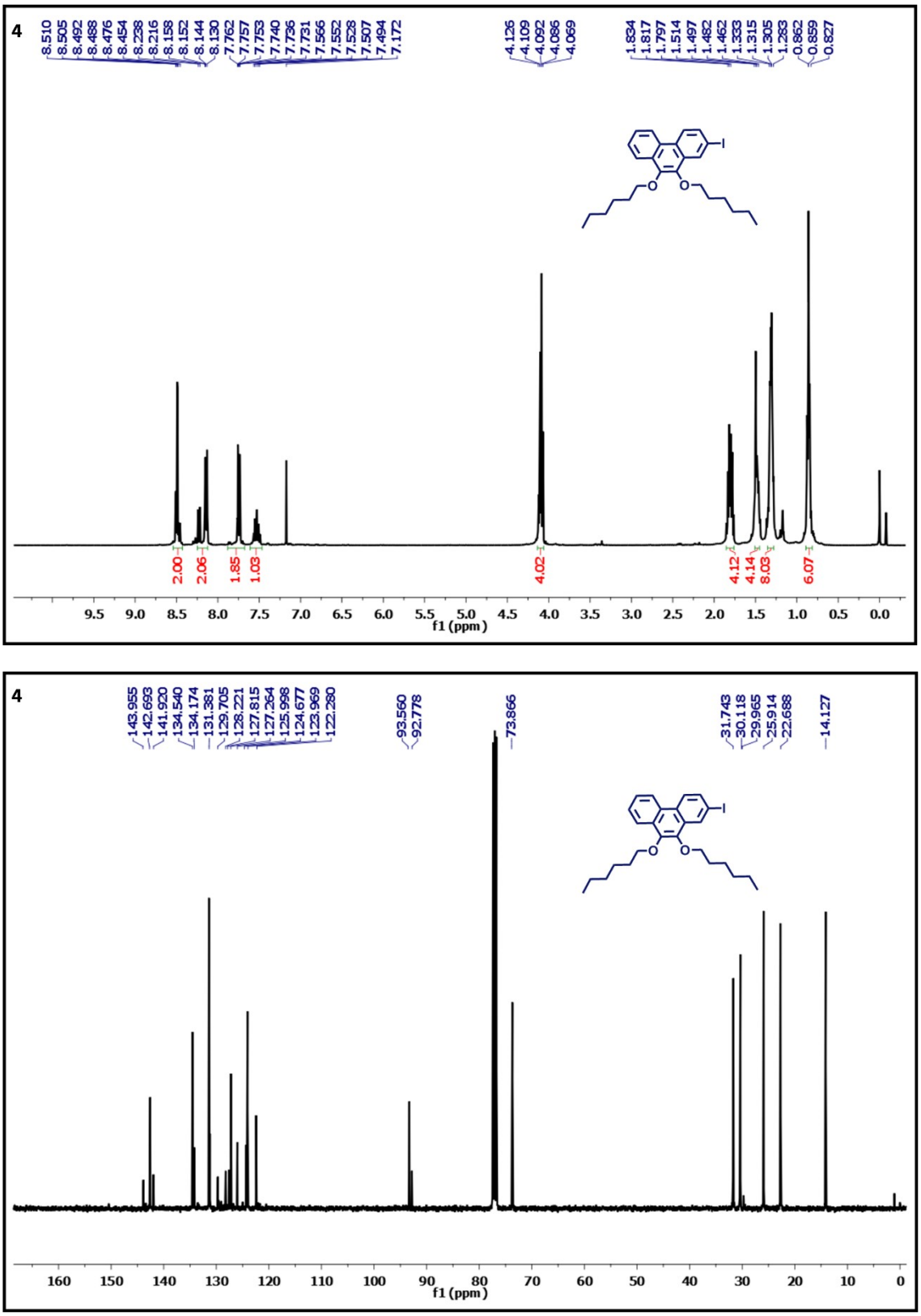

Figure S2: ^{1}H and ^{13}C NMR spectra of compound **4**

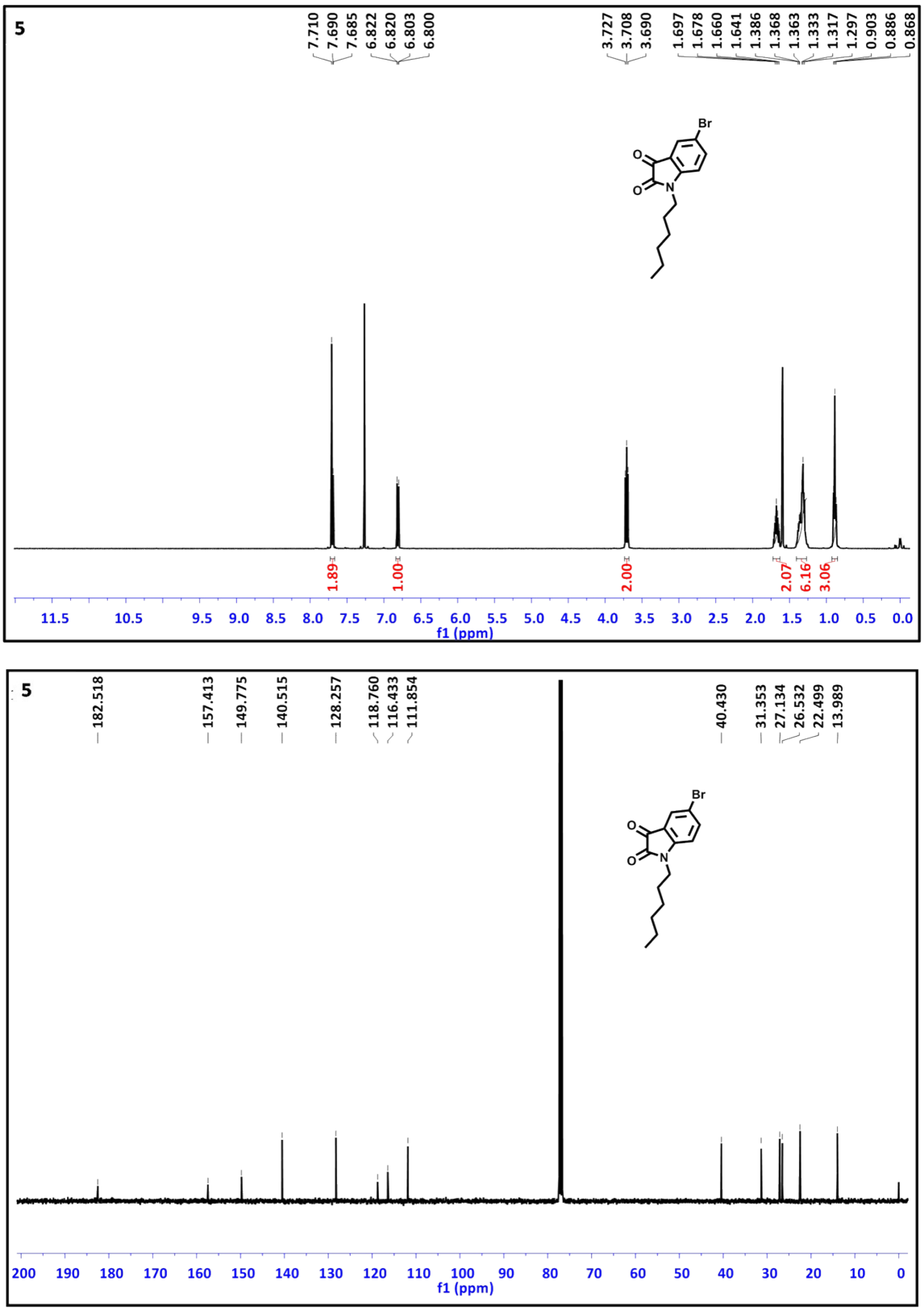

Figure S3: ^{1}H and ^{13}C NMR spectra of compound **5**

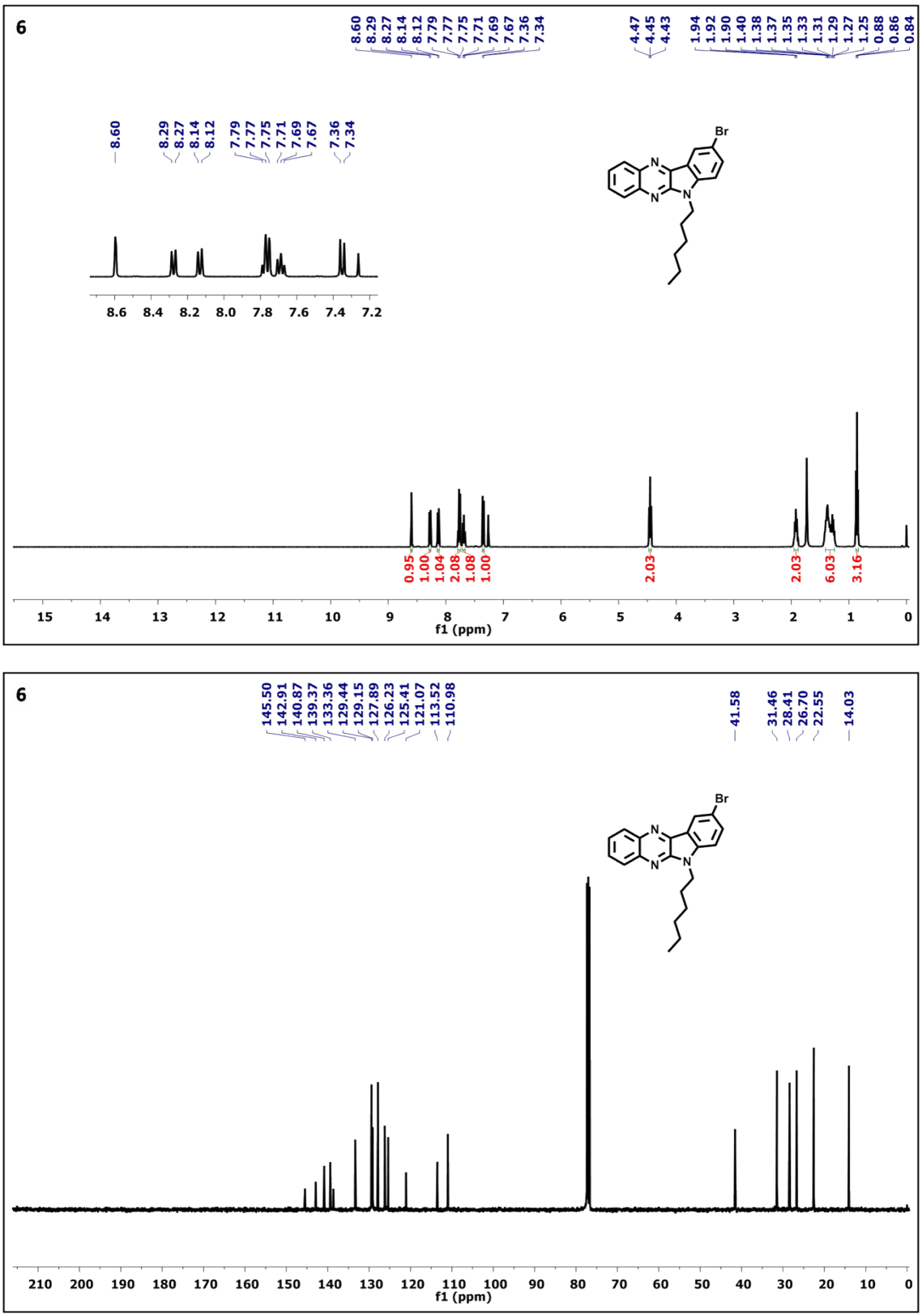

Figure S4: ^{1}H and ^{13}C NMR spectra of compound **6**

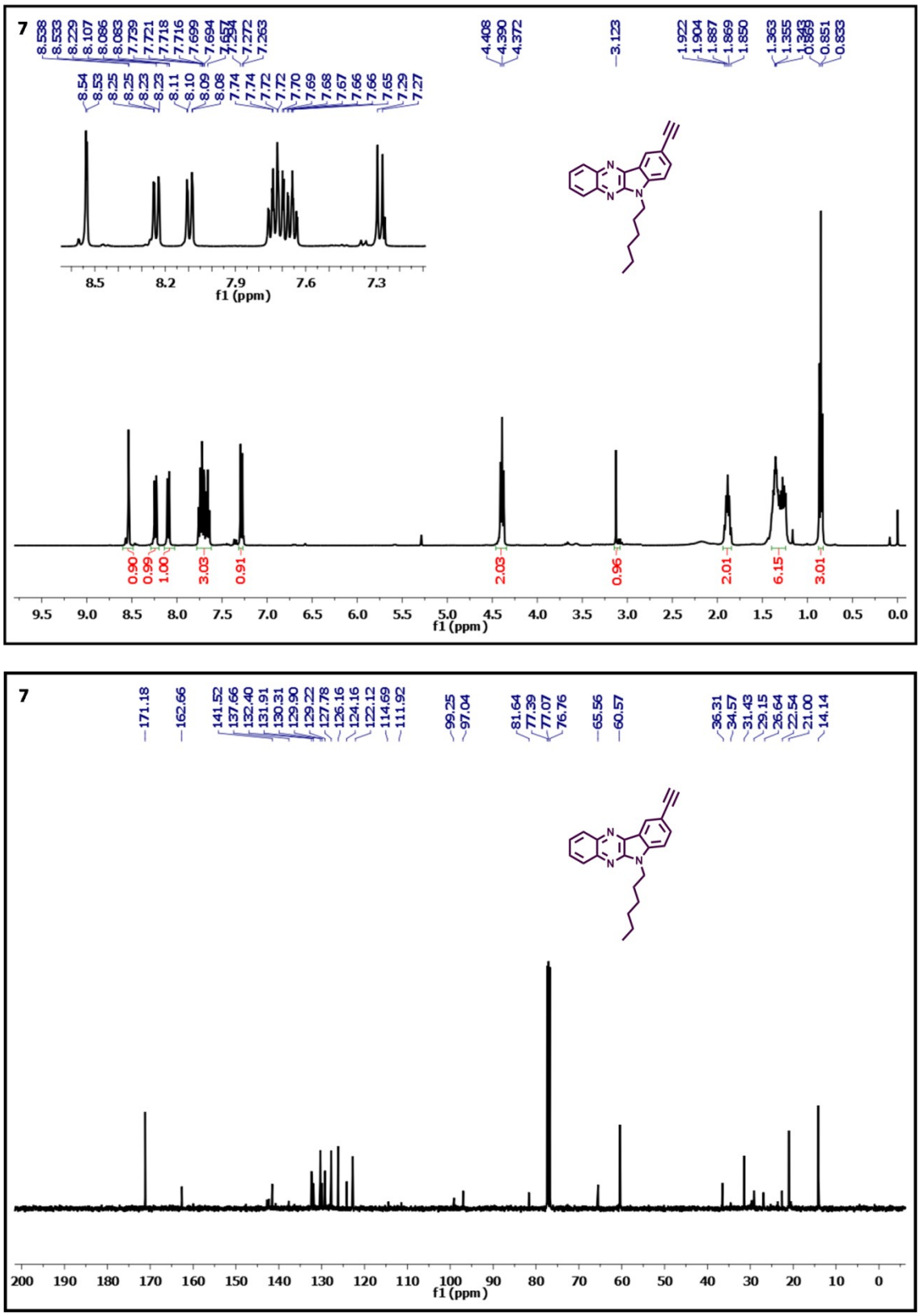

Figure S5: ^{1}H and ^{13}C NMR spectra of compound **7**

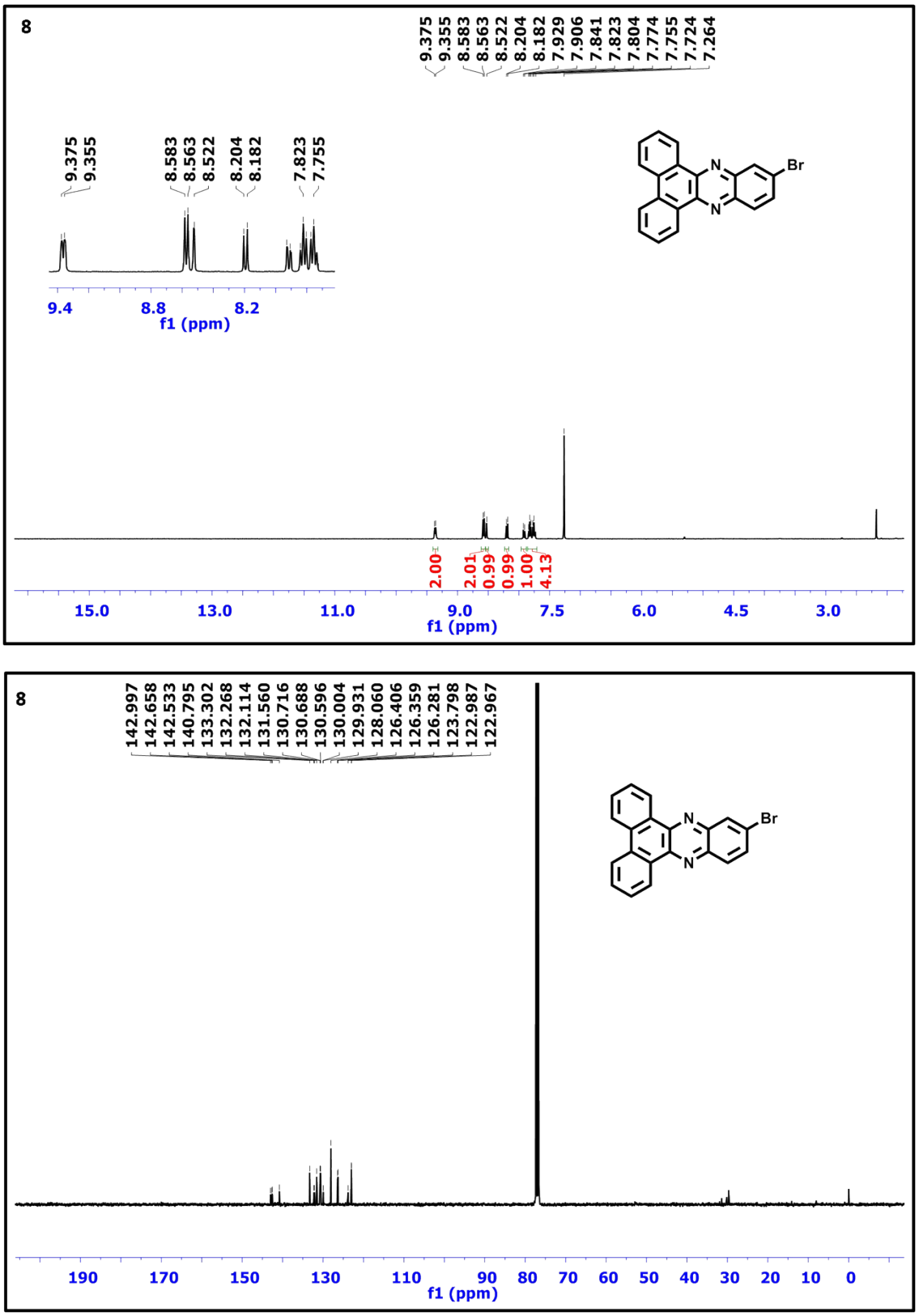

Figure S6: ^{1}H and ^{13}C NMR spectra of compound **8**

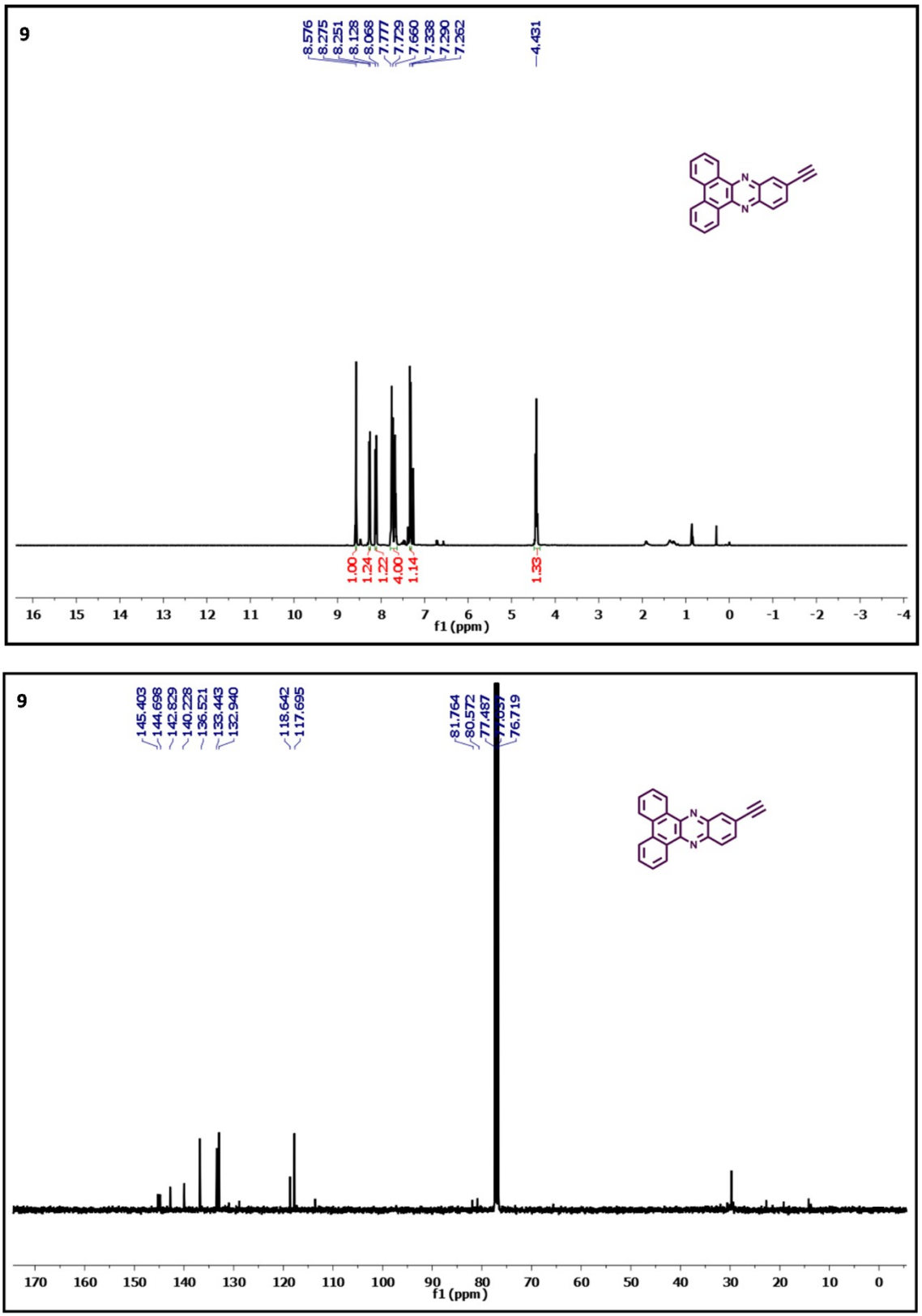

Figure S7: ^{1}H and ^{13}C NMR spectra of compound **9**

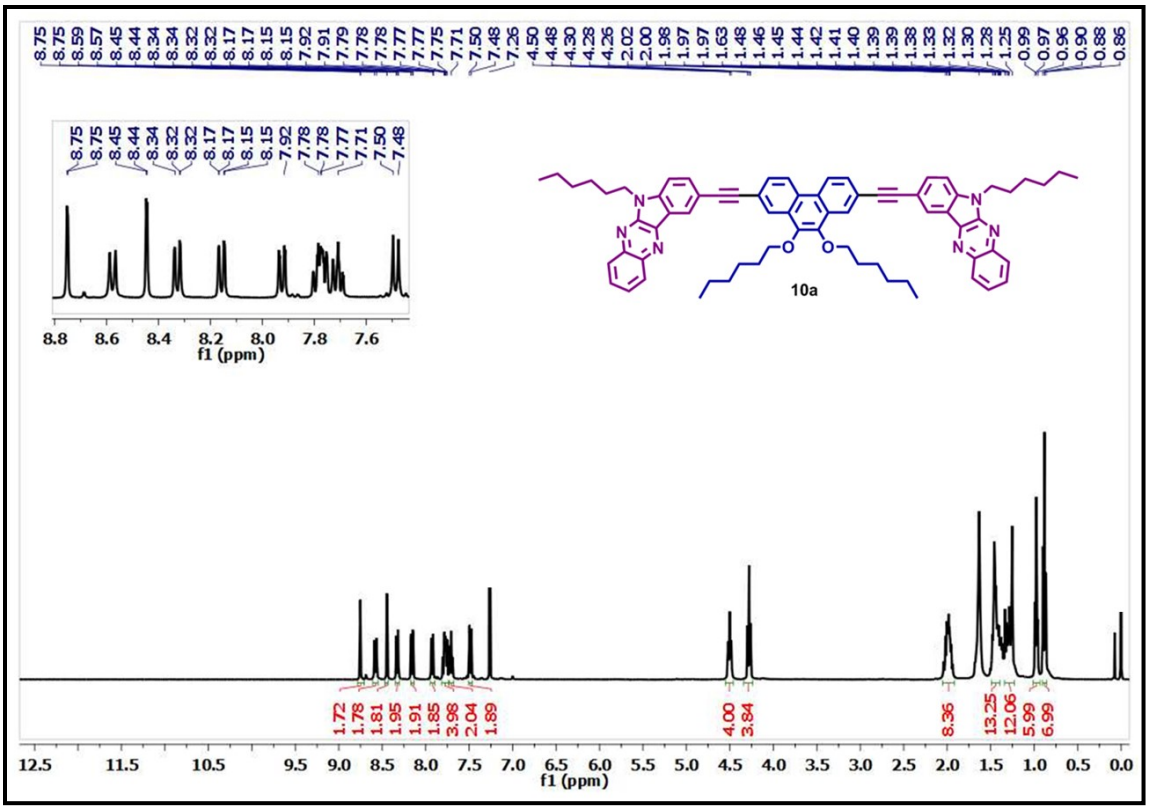

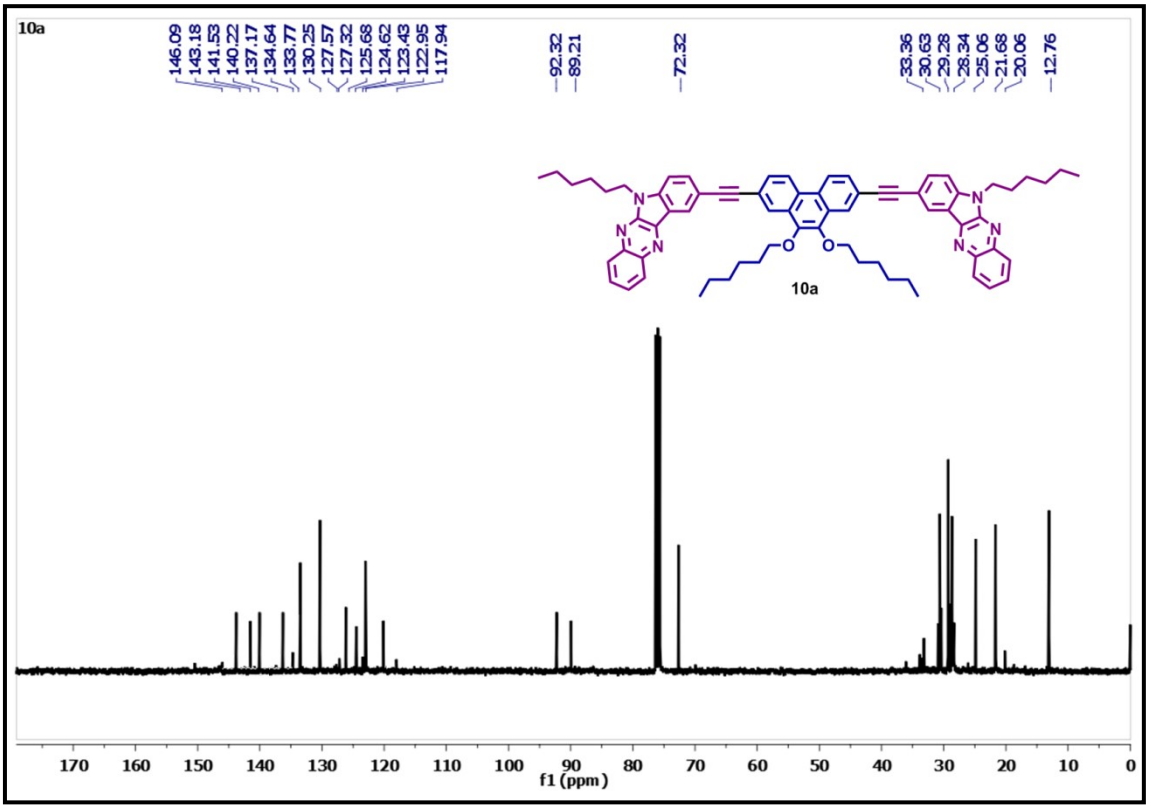

Figure S8: ^{1}H and ^{13}C NMR spectra of compound **10a**

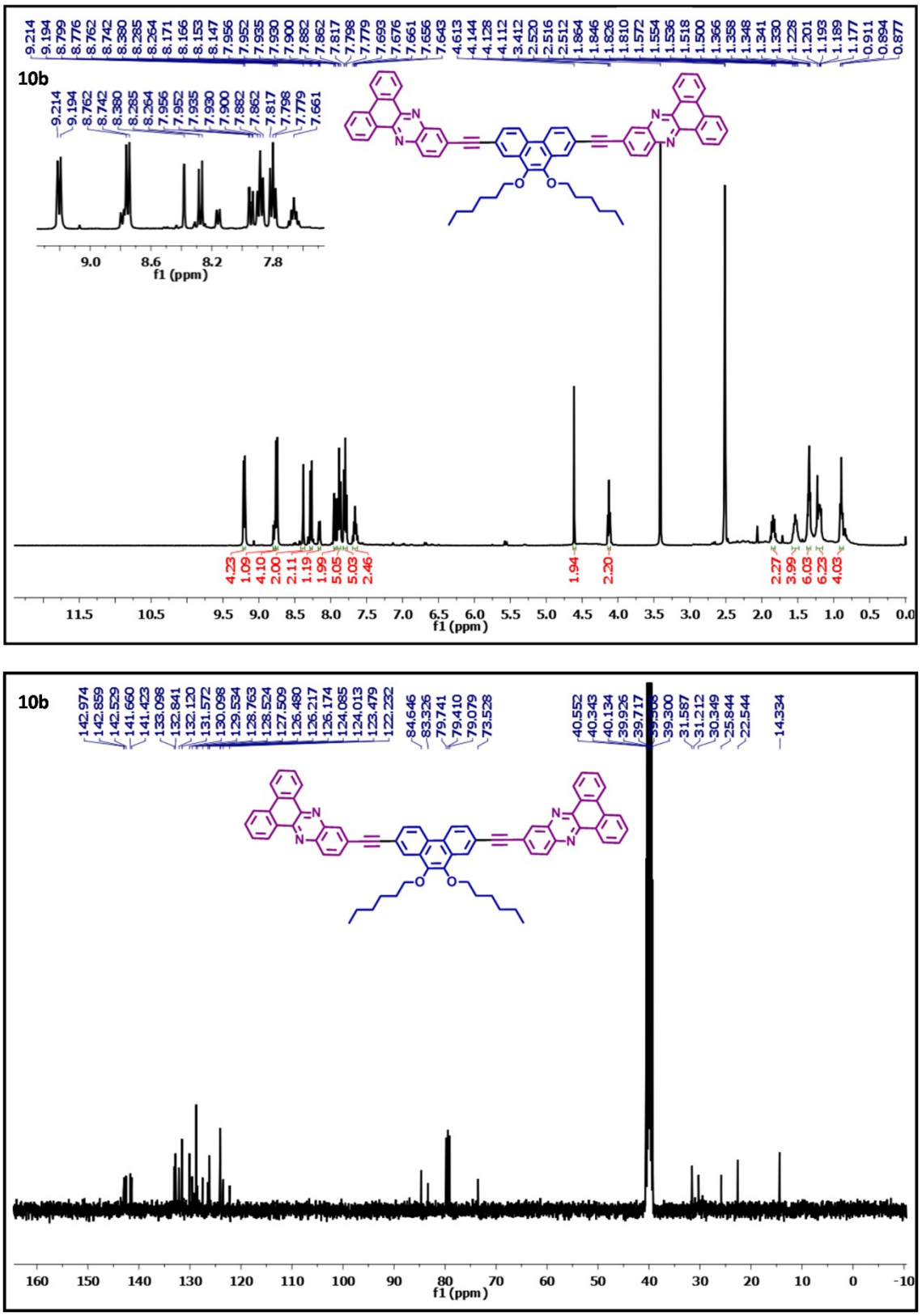

Figure S9: ^{1}H and ^{13}C NMR spectra of compound **10b**

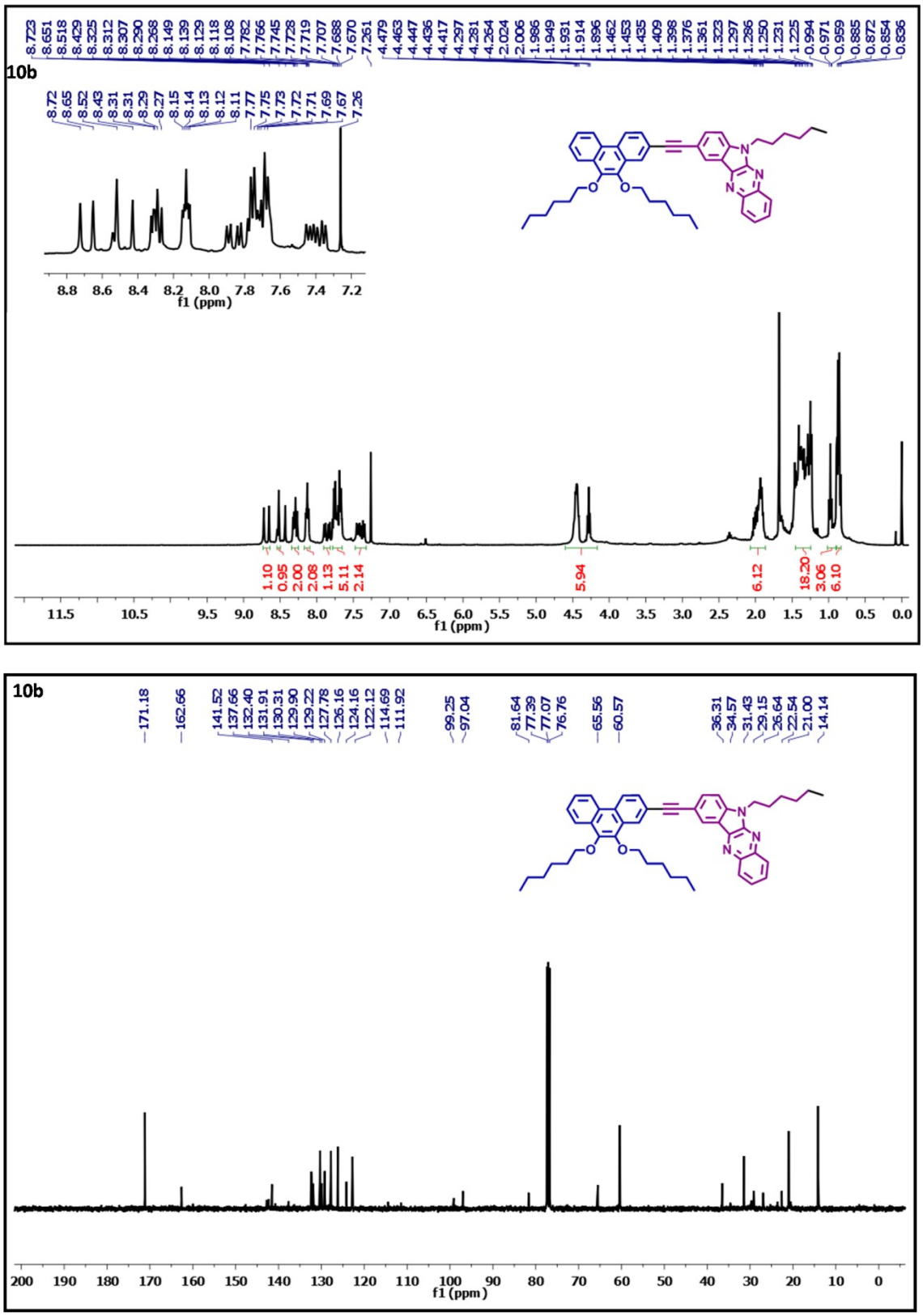

Figure S10: ^{1}H and ^{13}C NMR spectra of compound **11a**

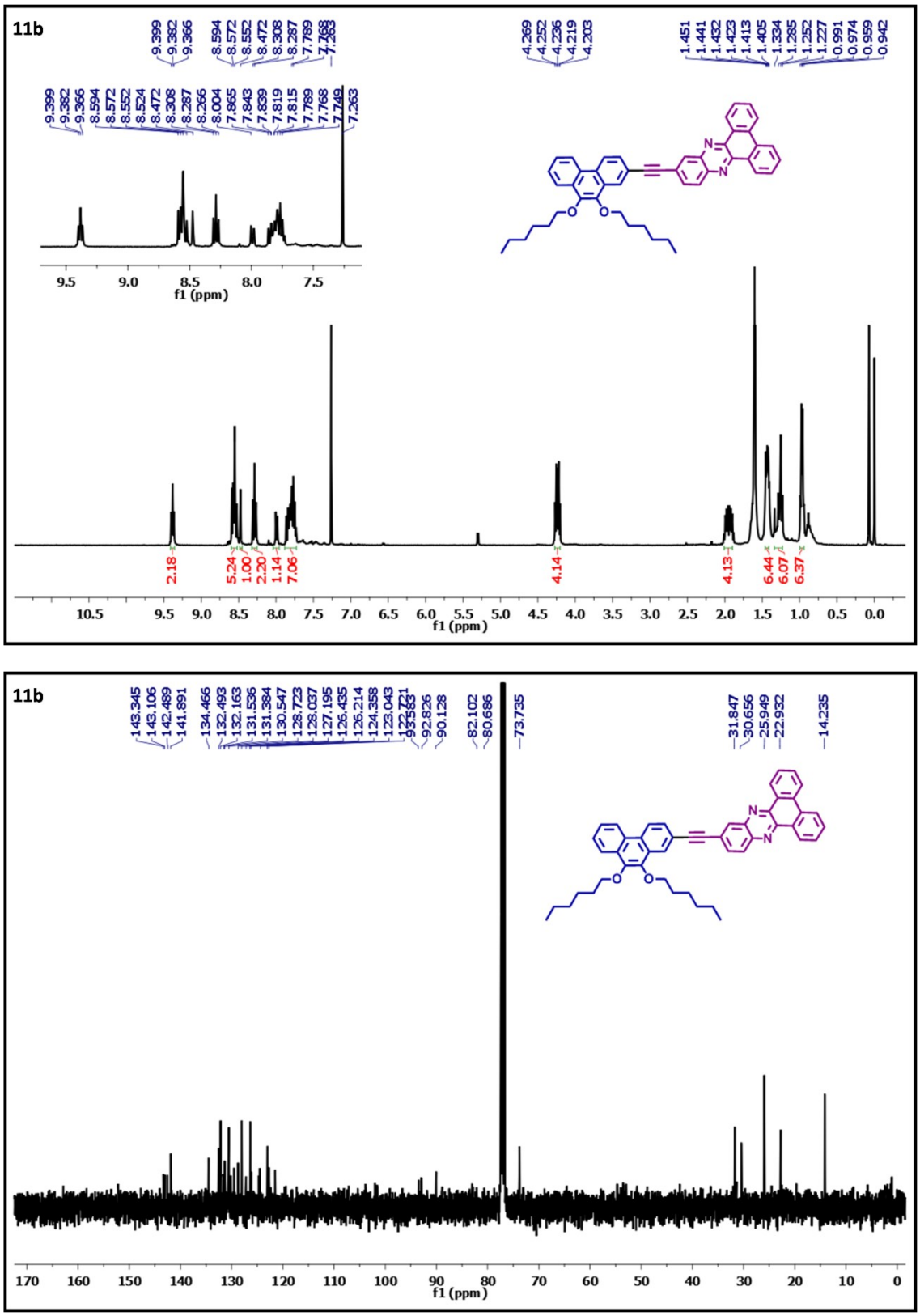

Figure S11: ^{1}H and ^{13}C NMR spectra of compound **11b**

5. HRMS spectra of the compounds 10a-b and 11a-b

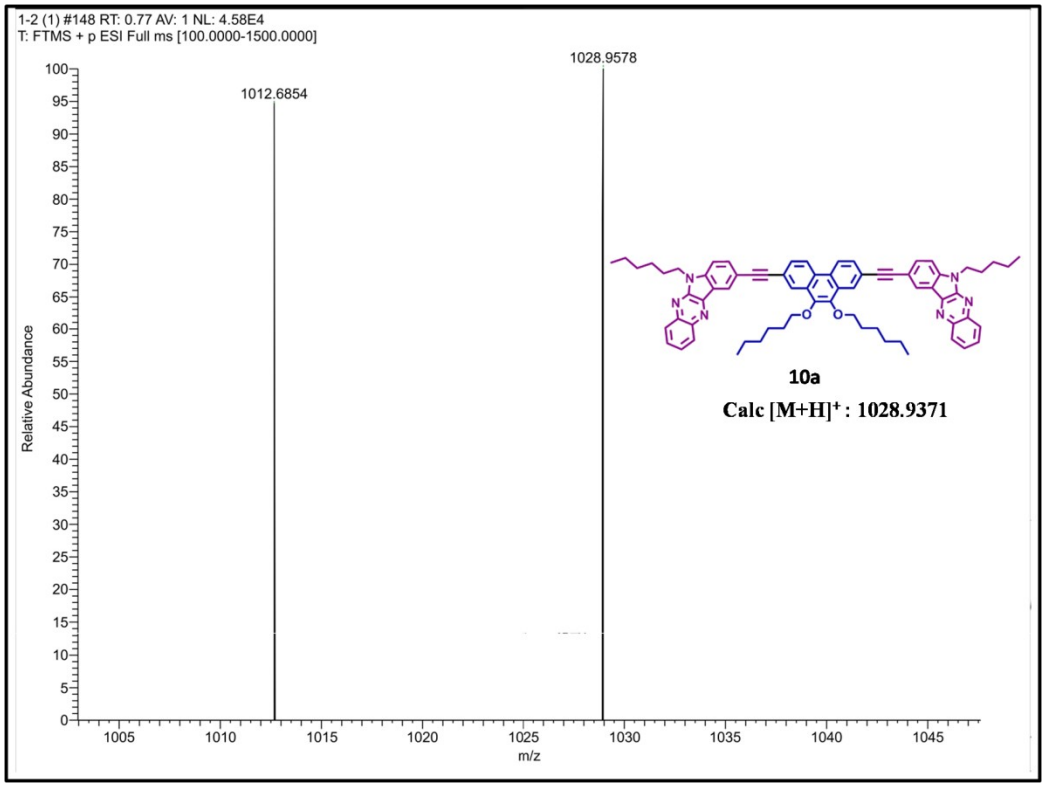

Figure S12: HRMS spectra of the compound **10a**

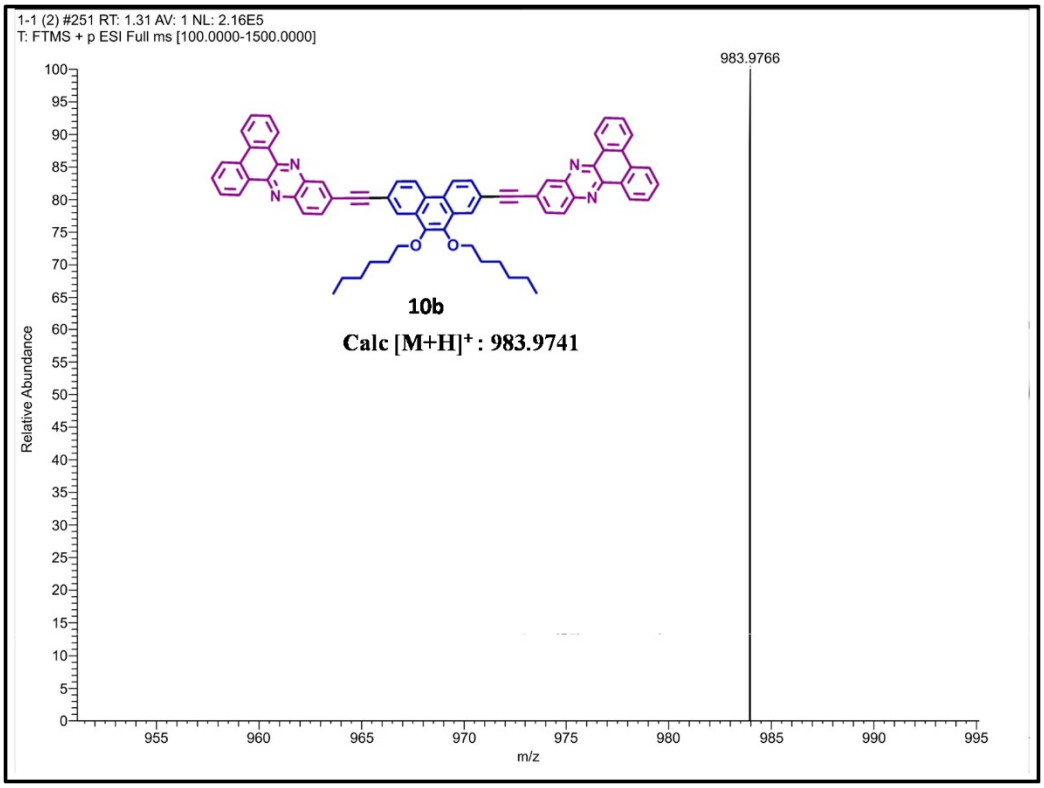

Figure S13: HRMS spectra of the compound **11a**

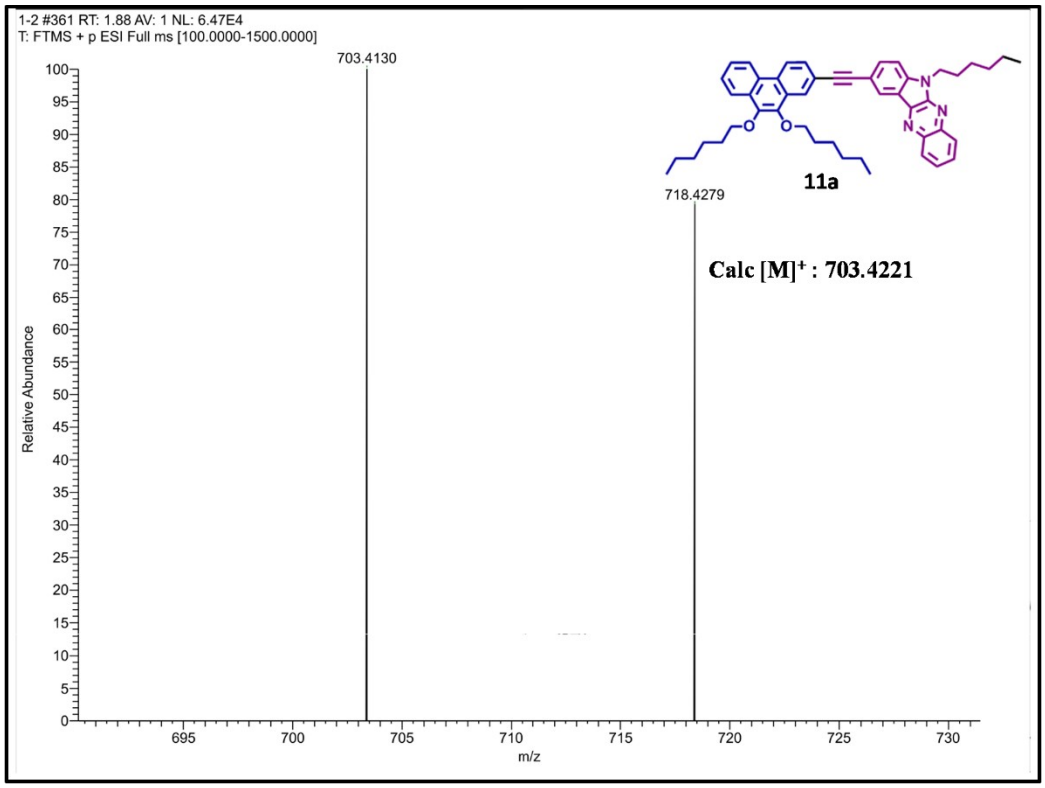

Figure S14: HRMS spectra of the compound **11a**

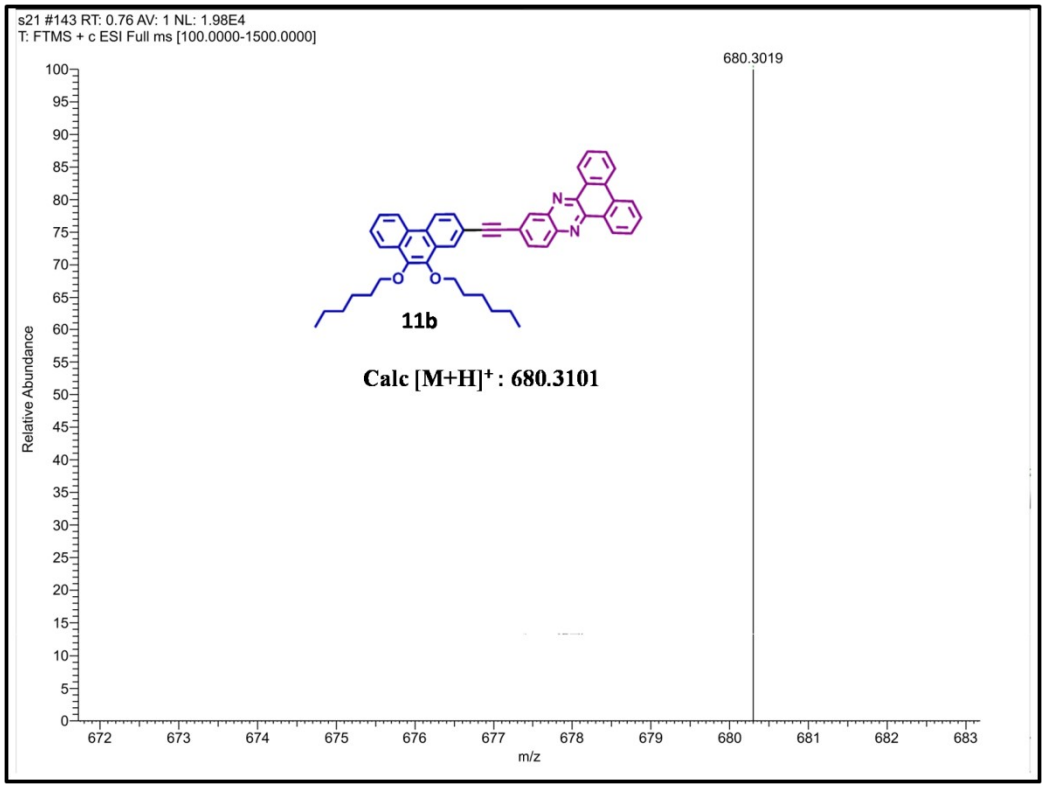

Figure S15: HRMS spectra of the compound **11b**

6. Thin film analysis of compounds 10a-b and 11a-b

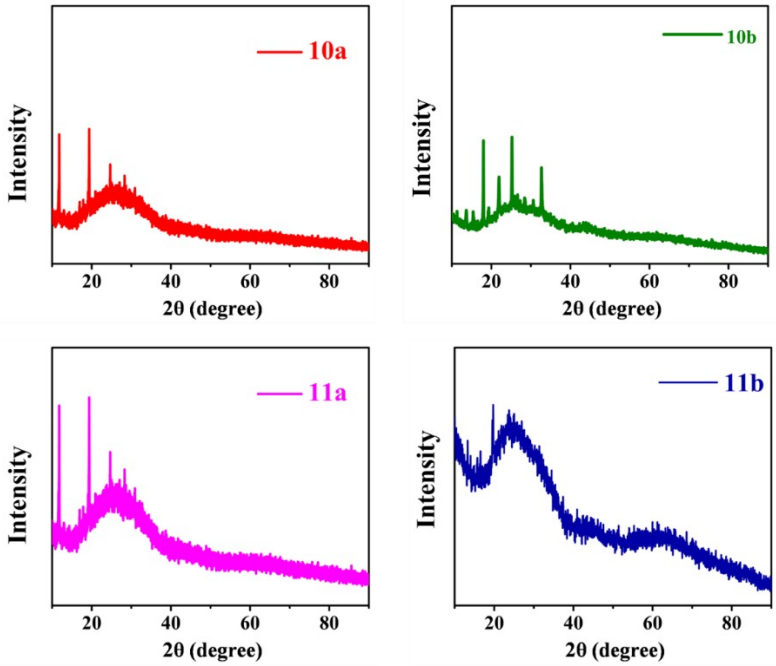

Figure S16: Thin-film XRD pattern of the synthesized compounds **10a-b** and **11a-b**

Table S1. Thin film analysis data of the compounds 10a-b and 11a-b

Compound	2θ	d-spacing (nm)	D (nm)	Crystallite size D_M (nm)
10a	11.74 19.69 24.65	0.753 0.450 0.361	28.61 28.89 35.64	31.04
10b	17.99 19.34 25.08 32.70	0.493 0.458 0.354 0.273	28.64 26.13 29.26 24.77	27.2
11a	11.74 19.69 24.65 28.28	0.753 0.450 0.361 0.315	28.61 28.89 35.64 30.47	30.90
11b	13.28 15.72 19.69	0.666 0.563 0.450	32.22 29.06 22.77	28.02

7. Electrochemical studies of the compounds 10a-b and 11a-b

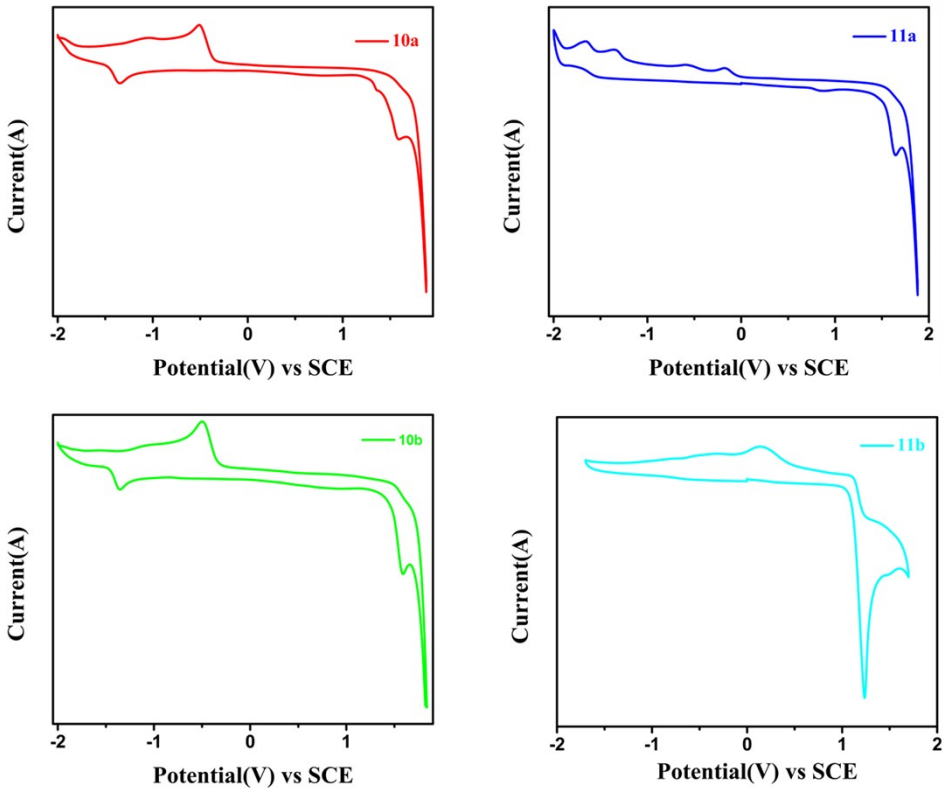

Figure S17: Cyclic voltammograms of the compounds **10a-b** and **11a-b**

8. Computational studies of the compounds 10a-b and 11a-b

A series of computational simulations, such as Molecular Mechanics and semi-empirical methods, were used to arrive at the plausible stereochemistry of the structure, as it is an essential aspect for packing and predicting molecular electronic properties of the system, some of which are usually non-covalent. These optimal geometrical parameters were then used to compute the optimized structure at the DFT's B3LYP level of theory and TD-SCF for spectral estimation theoretically using *Gaussian*.

The FMOs were visualized using GaussView. The optimized geometry was then used as input geometry for Density of States (DOS) calculations using *VASP (MedeA)* software. However, the structures were evaluated using solvent correction parameters such as GGA-PBE (basis set), and the DOS graphs were subsequently obtained. The Fermi Energy and band gaps were also computed. The density and volume of the cell were also computed. All the molecules pertained to a simple *Orthorhombic* System. The crystallographic values obtained from VASP were then used

to assign the crystal parameters and set up the packing pattern inside the *Discover Studio* Software. The packing patterns were modeled with various group symmetry elements, and only those that gave plausible parameters and hopping values were computed. These values are included in the table. The DFT calculations were performed with Gaussian at the 6- 31D level of theory **(Table S2)**. [1–3]

Table S2: Energy level of the synthesized molecules through DFT calculations and experimental results

C. No	HOMO (eV) DFT	HOMO (eV) Expt	LUMO (eV) DFT	LUMO (eV) Expt	Band Gap DFT	Band Gap Expt	Total Energy DFT (Hartrees)	Dipole D	Symmetry
10a	-5.083	-5.806	-1.961	-2.597	3.123	3.209	-3189.81	2.7067	C2
10b	-5.422	-5.853	-2.424	-2.622	2.998	3.231	3069.46	0.7049	C2
11a	-5.211	-5.793	-1 .946	-2.433	3.264	3.360	-2175.76	1.5407	C1
11b	-5.475	-5.447	-2.315	-2.143	3.159	3.304	-2115.59	1.1338	C1

Theoretical band gap values present a contrasting insight into our molecules, suggesting good transportability of electrons or holes when compared to experimental ones. **11a** has the highest band gap, followed by **10b** and **10a**. **10b** has the least band gap. These values are quite agreeably closer to the experimental ones. While the HOMO values calculated theoretically are closer to the experimental values, the values for LUMO differ slightly, but the overall difference in the FMO's is almost similar. To account for the discrepancies, solvent correction was incorporated in the VASP calculation where DFT-B was used, and the Fermi Gap (E Fermi) (**Table S4**) was computed. Here, it can be seen that the values and trends are agreeable **(Table S4)**. The Density of States (DOS) represents the number of states that offer high space for particle movements (**Figure S18**). Here, it can be seen that **10a** has the lowest DOS gap value, which does not agree with the experimental values. The Fermi gaps represent the availability of space for the movement of electrons at the molecular level, and the value of 2.86 for **10b** is in trend with the DFT values, which means that it offers the highest degree of mobility for the particle carrier. This molecule also has the lowest band gap predicted by the DOS (1.834). The compound **10b** has the least dipole

moment. The difference in values is only lighter as the type of calculation is explained in the methodology section.

Table S3: Experimental and computational absorption wavelength

Compounds	Experimental		Computational	
	Absorption λ_{max} (nm)	**Emission λ_{em} (nm)**	**Electronic Transition**	**Wavelength (nm)**
10a	426 356 291 267	513	S_0-S_1 S_0-S_3 S_{-2}-S_1 S_{-1}-S_3	452.9 397.5 371.3 345.5
10b	360 329 267	490	S_0-S_1 S_{-2}-S_1 S_{-4}-S_1 S_{-2}-S_2	464.8 396.1 383.9 377.2
11a	417 353 292 266	512	S_0-S_1 S_{-1}-S_2 S_0-S_2 S_{-4}-S_1	445.3 360.3 352.1 300.4
11b	359 332 264	523	S_0-S_1 S_{-3}-S_1 S_{-1}-S_2 S_0-S_3	437.9 357.4 341.6 307.6

The excited states of this series of molecules are calculated using a computational method and are compared favourably with experimentally obtained values. The TD-SCF (Time Dependent SCF) theoretical calculations suggest significant spectral insights. The bands found in the Experimental methods agree with the theoretical calculations. Also, the emission Spectrum values are quite predictable. The table shows the comparison, and out of the several values predicted by the theoretical methods, four values have been chosen that are closer to the experimental ones and have a good frequency factor. Inter-system crossing has been predicted in almost all the systems, and some of the values of Emission Spectra agree with these values. These are the states where excited electrons may be promoted to account for the spectral and conducting properties of the molecule. The TDDFT calculations also show various such states within the experimentally measured values. The series of FMOs present LUMO at the TOP and HOMO at the bottom, and from these, it can be observed that less localization is there in the central part of the molecule in

the HOMO's and more of it in the LUMOs'. However, the combination of the orbital phases varies on moving from HOMO to LUMO. This should make transporting or switching electrons/particles within the vicinity easier. Given the low band gaps for these two, it is now evident, both from experimental and theoretical calculations, that they serve as better switching devices.

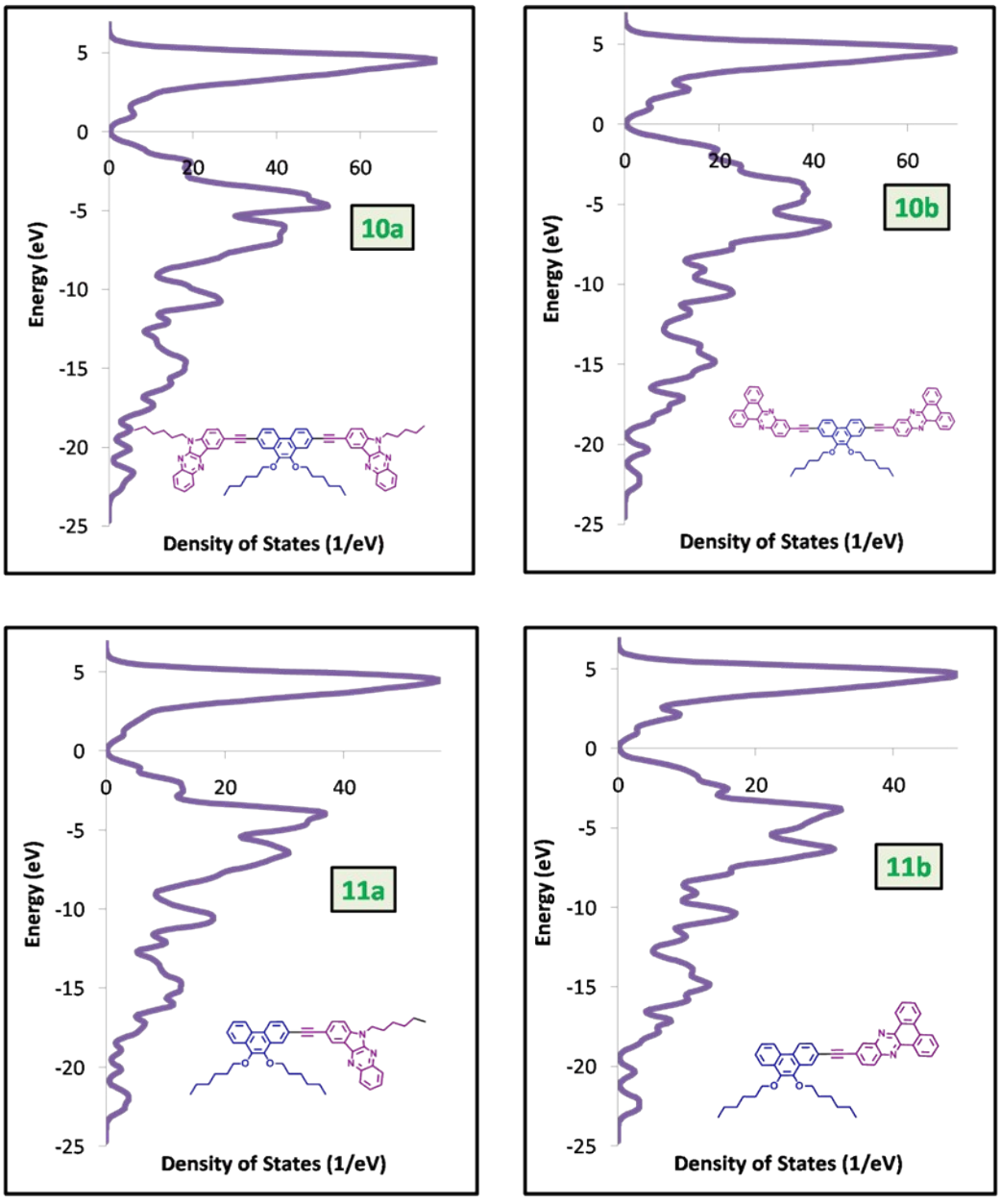

Figure S18: DOS graphs of the compounds **10a-b** and **11a-b**

All the molecules transition from very low levels to some higher levels have been observed, and it has been found that the molecules have transitions among the core part rather than the side

chains, but the orbital only seems to have different orientations along different coordinates. With very low band gaps, all transitions can be accounted for and compared with experimental values. Transitions from lower HOMO (like S_{-4}) to LUMOs have been observed in almost all the cases, but very low have been found with the **10b** derivative. The electronic effects of the substituent might have affected this transition in **11b**.

Table S4: VASP calculations of the synthesized compounds 10a-b and 11a-b

Compound	Molecular Formula	Free Energy eV	Density (mg/m^3)	DOS Gap (eV)	Band Gap (eV)	E Fermi (eV)
10a	$C_{70}N_6O_2H_{72}$	-958.572	0.157	1.838	2.959	-3.353
10b	$C_{70}N_4O_2H_{54}$	-874.289	0.118	1.834	2.846	-3.836
11a	$C_{48}N_3O_2H_{53}$	-666.158	0.144	1.965	2.974	-3.369
11b	$C_{48}N_2O_2H_{44}$	-624.025	0.154	1.988	2.987	-4.506

This has been shown in the packing of the molecules in another section. A detailed quantitative study of the orbitals involved in transition with symmetry-labelled levels is possible, but beyond the scope of this article, as it would take up much space. This kind of transition has been considered a characteristic of good particle transport. A generalization to this phenomenon has been summarised by Martin *et. al*[4] where the relaxation time has increased upon an electron-donating substituent (or delocalization).

Table S5: Packing and cell parameters of the synthesized molecules

Compound	Cell Parameters	Type of the Cell	Preferences	Symmetry	Hopping Distances (Å)
10a	15.2/37.3/19.2 90/90/90	simple orthorhombic	1 1 3	PNA21	4.088 8.521 8.701
10b	20.2/39.6/17.2 90/90/90	simple orthorhombic	1 1 3	P212121	3.984 5.567 5.910
11a	26.3/18.2/16.9 90/90/90	simple orthorhombic	3 1 3	P21-c	4.955 7.760 8.132
11b	26.8/19.6/13.9 90/90/90	simple orthorhombic	3 4 1	P21-c	3.971 5.272 7.642

Apart from the properties computed, other factors such as specific heat, paramagnetic susceptibility, and solvent-dependent properties contribute to the overall expected functionality. Some selected transitions closer to the experimental values were visualized using the Gauss view. These orbitals are picturized in the table above to show the probable locations from and to where the transitions occur (**Table S3**). A quantitative approach regarding the substitution effect can thus be established.

on the prediction of crystal parameters by the MedeA, the packing of the molecules was taken up with Discovery Studio software, where the group symmetry was assigned and modelled. The hopping values were then found to account for non-covalent interactions that should stabilize the packing pattern. This packing also should allow one to observe the stacking factor as well. The Space groups were chosen to represent the plausible crystalline structure. While some inter-atomic distances were monitored and measured below 10 Å, other hopping distances calculated by the software were ignored to accommodate only the significant ones. It can be seen that the hopping distances are favourable enough for effective interactions within the given packing.

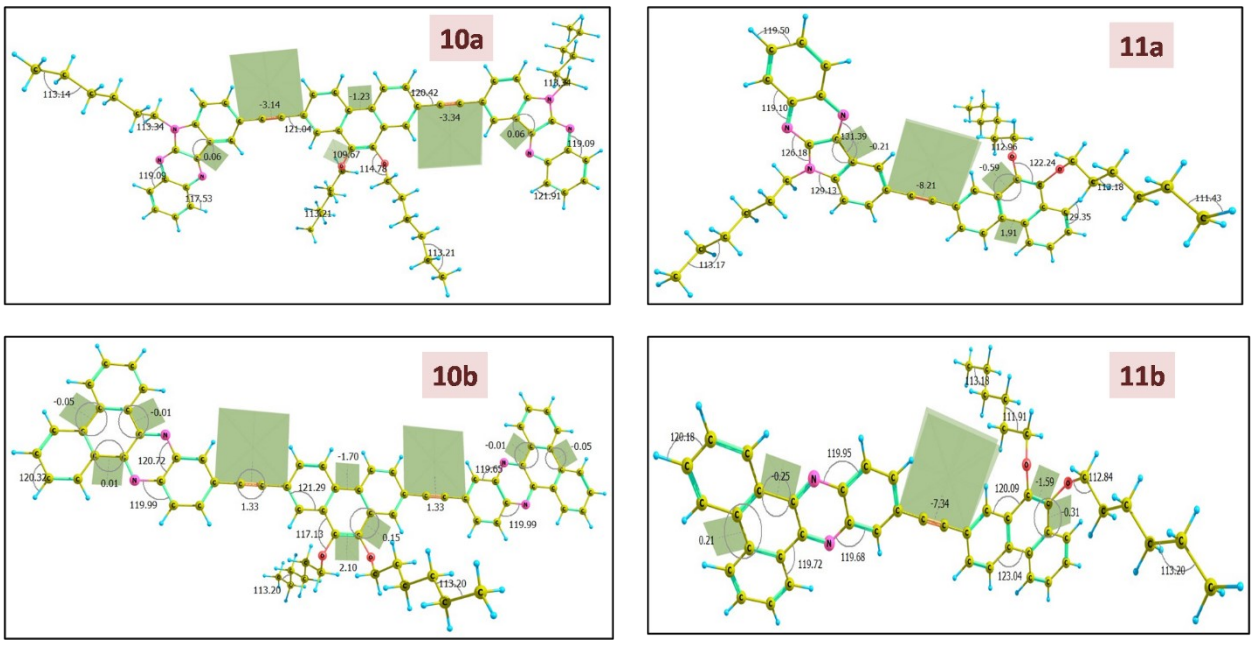

Figure S19: Optimized geometry of the compounds **10a-b** and **11a-b**

It can also be seen that the interacting distances for **10b** and **11b** are as low as 3 Å, and such closer inter-atomic stabilisation could substantiate the properties we are looking for. Various symmetry structures were tried to obtain the packing pattern for the molecule, but closer interaction and stabilization were found only with the respective symmetry mentioned in the **Table S5**. For

instance, for the **11a** and **11b** molecules in the series, P21 is the symmetry with which the structure appears to present a solid packing with more stabilization due to inter-atomic interaction with corresponding hetero atoms. The other **10a** and **11a** molecules have different packing symmetries, allowing molecular packing in a favourable pattern for intermolecular interaction and supporting the polymorphic structure. Such a packing with minimum repulsion and maximum interaction with plenty of orbitals makes this molecule suitable for molecular switching devices.

Molecular packing of the synthesized molecules 10a-b and 11a-b

Compound 10a:

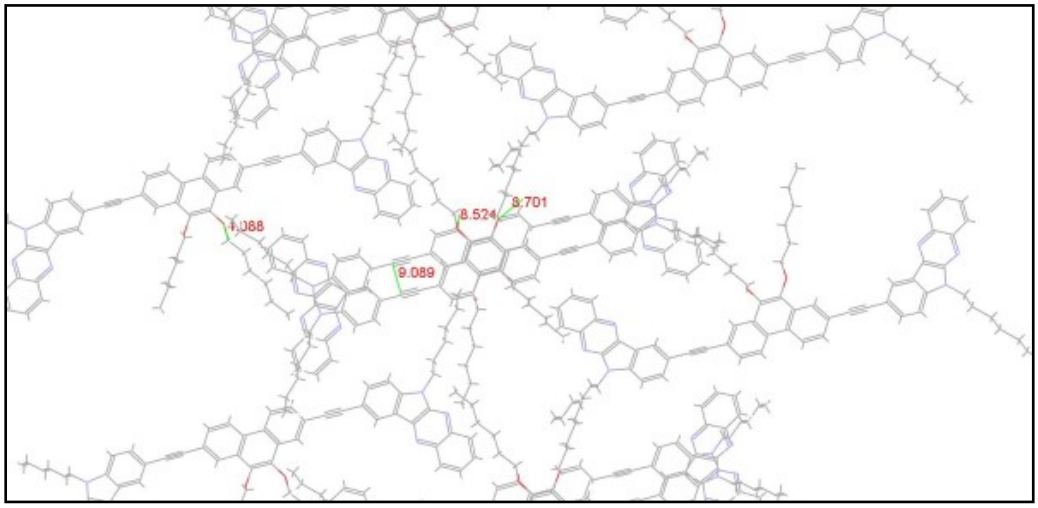

The phenanthrene part of the molecule with a longer alkyl chain was found to stabilize the crystal packing at a distance sufficient for accounting for non-covalent interactions and is supported by several hetero atoms like O and N. The acetylene moieties were not placed closer to offer pi-pi stacking but had distances within 10 Å. The molecules were packed in such a manner that the central part of one unit was tilted by an angle of about 110º due probably to the steric factors offered by the alkyl attachment. In all the packing, it was found that several interactions stabilized it and gave it the appearance of a fish skeleton.

Compound 10b:

One end of the indole-quinoxaline is found packed over another end of the same moiety of the next molecule so that extended alkyl chains appear quite opposite to each other and give an appearance of a collapsible x-pattern with each H-atom lying opposite to the other of the same molecule's another tail (alkyl). These are stabilized by about 5.9 Å and 5.5 Å non-covalent interactions. There are other interactions as well.

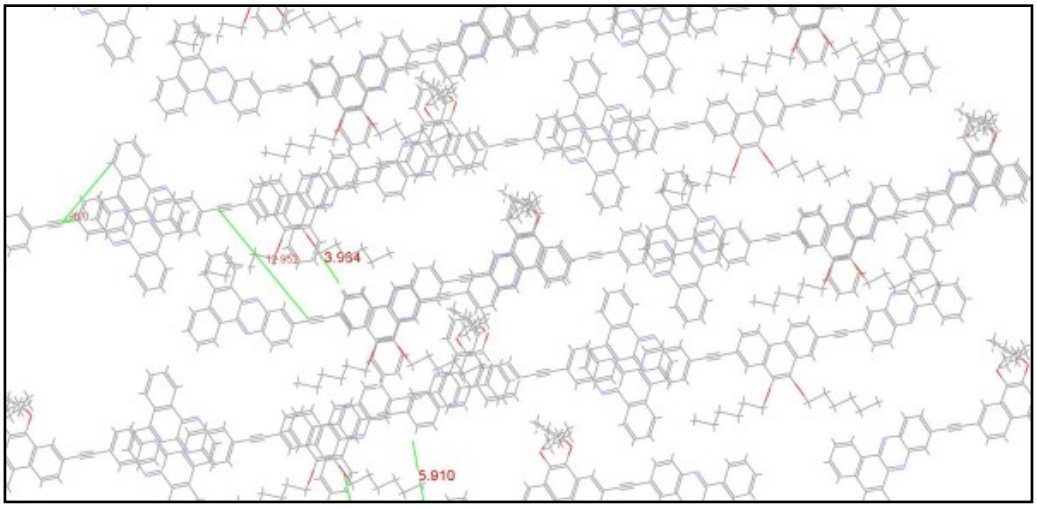

For instance, a H-atom at the end of a molecule is found to interact with the O-atom of the tailing side chain of the next molecule at about 3.9 Å. The pi-pi interactions are not possible as they are at about 12.9 Å minimum. Overall, this symmetry packing gives a beautiful crystalline structure.

Compound 11a:

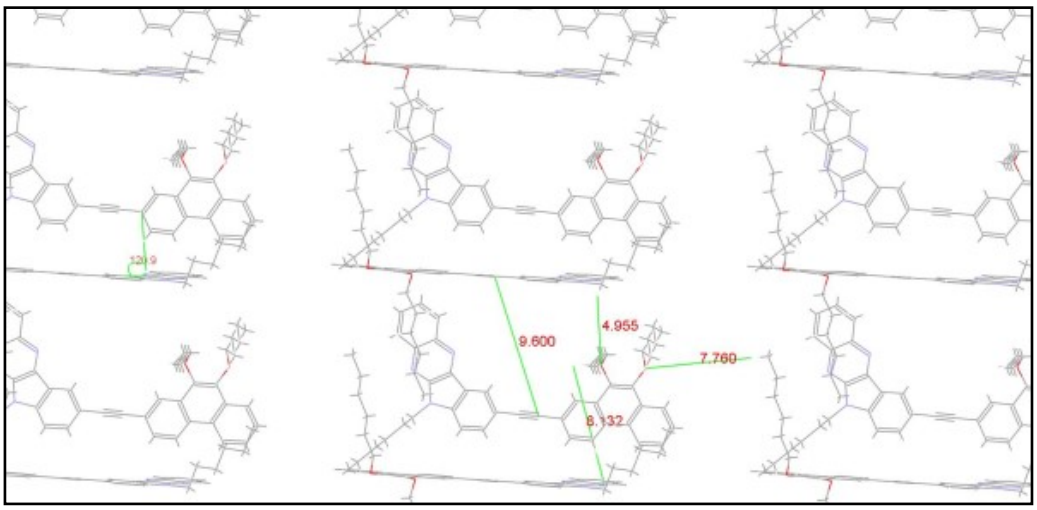

The planarity of the entire molecule was disturbed by heavier substitution. The twist of alkyl substitution at the phenanthrene moiety was found to stabilize with other adjacent units by several interactions (4.9 and 7.7 Å). The presence of acetyl groups did not give rise to effective pi-pi stacking as the molecule was found to be strained, and the distance was about 9.6 Å. The molecules were also packed in a twisted pattern, and the entire packing appeared to be a crisscross pattern all over the system.

Compound 11b:

The molecules are packed so that their planes are about 138° to each other, unlike the previous molecule, where each was parallelly placed over the other. As a result, the pi-pi interaction is possible (at a distance of about 7.6 Å here). Other interactions include O and N- and based ones in a distance of about 5.2 and 3.9 Å, between the alkyl side chain and the planar H atoms of the next molecule.

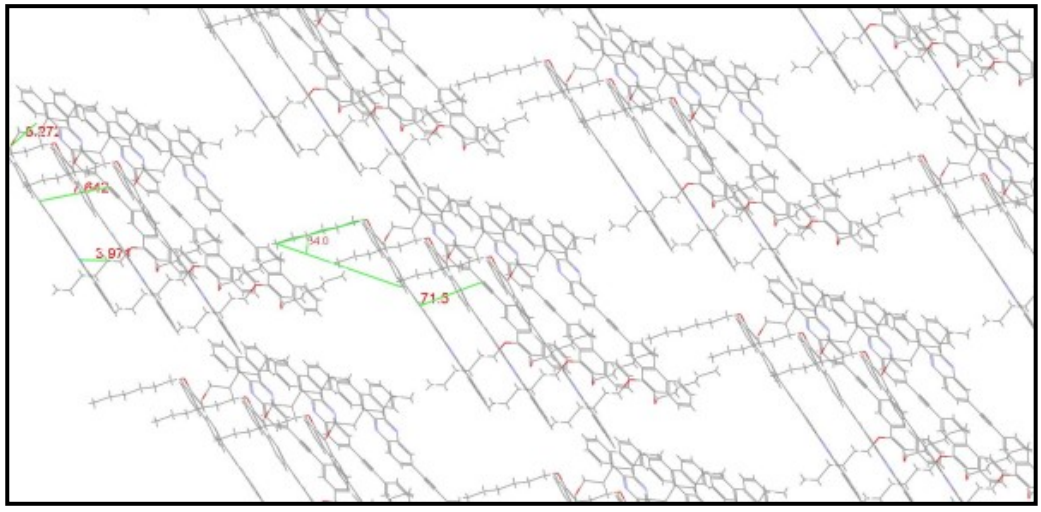

This type of stabilization has given rise to a highly planar surface for a layer of the molecules, giving a needle-like structure at a particular dimension. This extends over the entire length of the molecule.

9. Memory device fabrication

All the devices were fabricated on the cleaned and patterned ITO-coated glass substrates (Highly transparent ITO, with surface resistivity 8-12 Ω/sq). ITO-coated glass substrates were sequentially cleaned with distilled water, isopropanol, and ethanol by sonication for 20 min in each solution. The synthesized compounds were dissolved in chloroform at a concentration of 3 $mgmL^{-1}$. The as-prepared solution was spin-coated over the cleaned ITO-coated glass substrate at 1200 rpm. After 20 minutes of annealing on a hot plate at 80 °C, the residual solvent was eliminated. Then, the active layer-coated substrates were cooled down to room temperature. Later, the Ag electrode was deposited on top of the semiconducting layer using the sputter coating technique through a shadow mask of 1 mm in dimension. The device was then utilized to examine I-V characteristics.

A Keithley 4200A SCS analyzer was used to investigate memory characteristics. A probe station was utilized to source a voltage and simultaneously read the associated current. The SMUs were

connected to a probe station (Everbeing), consisting of two test probes and micro-positioners (made up of tungsten). Test probes could be adjusted in various directions with the micro-positioners, which allowed the measurements to characterize the memory device parameters.

References:

[1] S. L. Price, *Int. Rev. Phys. Chem.***2008**, *27*, 541–568.
[2] M. Shamsipur, A. Siroueinejad, B. Hemmateenejad, A. Abbaspour, H. Sharghi, K. Alizadeh, S. Arshadi, *J. Electroanal. Chem.***2007**, *600*, 345–358.
[3] B. Attar, Kubaib; Predhanekar, Mohammed Imran, A. Aathif, *Comput. Theor. Chem.***2022**, *1217*.
[4] M. Bracker, F. Dinkelbach, O. Weingart, M. Kleinschmidt, *Phys. Chem. Chem. Phys.***2019**, *21*, 9912–9923.